Combining controlled-source seismology and receiver function information to derive 3-D Moho topography for Italy

M. Spada,[1] I. Bianchi,[2] E. Kissling,[3] N. Piana Agostinetti[4] and S. Wiemer[5]

[1]*Laboratory for Energy Systems Analysis, Paul Scherrer Institute, Villigen PSI, Switzerland. E-mail: matteo.spada@psi.ch*
[2]*Institute für Meteorologie und Geophysik, Universität Wien, Vienna, Austria*
[3]*Institute of Geophysics, ETH Zurich, Zurich, Switzerland*
[4]*Dublin Institute for Advanced Studies, Dublin, Ireland*
[5]*Swiss Seismological Service, ETH Zurich, Zurich, Switzerland*

GJI Seismology

SUMMARY

The accurate definition of 3-D crustal structures and, in primis, the Moho depth, are the most important requirement for seismological, geophysical and geodynamic modelling in complex tectonic regions. In such areas, like the Mediterranean region, various active and passive seismic experiments are performed, locally reveal information on Moho depth, average and gradient crustal V_p velocity and average V_p/V_s velocity ratios. Until now, the most reliable information on crustal structures stems from controlled-source seismology experiments. In most parts of the Alpine region, a relatively large number of controlled-source seismology information are available though the overall coverage in the central Mediterranean area is still sparse due to high costs of such experiments. Thus, results from other seismic methodologies, such as local earthquake tomography, receiver functions and ambient noise tomography can be used to complement the controlled-source seismology information to increase coverage and thus the quality of 3-D crustal models. In this paper, we introduce a methodology to directly combine controlled-source seismology and receiver functions information relying on the strengths of each method and in relation to quantitative uncertainty estimates for all data to derive a well resolved Moho map for Italy. To obtain a homogeneous elaboration of controlled-source seismology and receiver functions results, we introduce a new classification/weighting scheme based on uncertainty assessment for receiver functions data. In order to tune the receiver functions information quality, we compare local receiver functions Moho depths and uncertainties with a recently derived well-resolved local earthquake tomography-derived Moho map and with controlled-source seismology information. We find an excellent correlation in the Moho information obtained by these three methodologies in Italy. In the final step, we interpolate the controlled-source seismology and receiver functions information to derive the map of Moho topography in Italy and surrounding regions. Our results show high-frequency undulation in the Moho topography of three different Moho interfaces, the European, the Adriatic–Ionian, and the Liguria–Corsica–Sardinia–Tyrrhenia, reflecting the complexity of geodynamical evolution.

Key words: Controlled source seismology; Crustal structure; Europe.

1 INTRODUCTION

The 3-D distribution of seismic velocities (seismic structure) is the most important parameter from which lithospheric structure and composition can be determined as well as to analyse tectonics. Furthermore, reference 3-D crustal models (e.g. Mooney *et al.* 1998; Bassin *et al.* 2000) are globally used to improve assessment of earthquake source parameters and they represent a prime *a priori* information for other seismological studies of the deeper earth.

For *P* and *S* velocity models, the geometry of the crust/mantle boundary, known as Moho, is the main first-order structure influencing the interpretation of seismic data from controlled-source seismology (CSS), local earthquake tomography (LET) and receiver functions (RF). The Moho separates the chemically highly differentiated crust from upper mantle. Thus, it is strongly correlated to tectonic processes and geodynamical evolution. As a consequence, the lateral variation of the velocities due to Moho topography, strongly distorts teleseismic wave fronts and influences teleseismic

traveltimes (Arlitt *et al.* 1999; Waldhauser *et al.* 2002; Sandoval *et al.* 2003). Hence, Moho topography has been used for tectonic and geodynamic modeling, to understand state and evolution of lithosphere, and it has been shown to be a prerequisite for the definition of reference 3-D crustal models for high-resolution teleseismic tomography (e.g. Lippitsch *et al.* 2003).

Over the years, seismic data have been interpreted with various techniques such as 1-D Herglotz–Wiechert inversion, 2-D ray tracing methods and synthetic seismogram modeling to estimate the location of seismic interfaces and associated velocities below the profile (e.g. Giese *et al.* 1976; Egloff 1979; Ye *et al.* 1995). The modeling results are usually presented in the form of seismic cross-sections along profiles enhancing the resolved parts of the model but without including quantitative error estimates for the derived structures (e.g. Brueckl *et al.* 2010). In a complex 3-D environment like the Alpine-central Mediterranean region, however, seismic data exhibits largely variable errors (Kissling 1993), mainly as a result of different acquisition and interpretation techniques.

In recent years, local reference 3-D crustal models for the greater Alpine region (e.g. Waldhauser *et al.* 2002) and south–central Fennoscandia (e.g. Sandoval *et al.* 2003), as input for high-resolution seismic tomography were developed based on the methodology described in Waldhauser (1996) and Waldhauser *et al.* (1998) where the construction of the crustal model is originally based on CSS profiles only. In Waldhauser *et al.* (1998), quantitative error estimate of Moho depths and topography are assessed to better constrain the Moho interface. The methodology described in Waldhauser *et al.* (1998) is straightforward and leads to high-quality 3-D reference crustal models (e.g. Arlitt *et al.* 1999).

Seismic refraction, near-vertical and wide-angle reflection experiments (CSS) are traditionally the most reliable and accurate seismic techniques in mapping the Earth's shallow lithosphere structure (Giese *et al.* 1976). These methods, however, require rather expensive seismic experiments. As a consequence there exists only a limited number of studies using these techniques on a global scale (Mooney *et al.* 1998). In Italy, after several decades of seismic exploration by the *Crosta Profonda* (CROP) consortium (Scrocca *et al.* 2003) and in the context of international research projects (e.g. Blundell *et al.* 1992), there exist a significant number of CSS profiles. With respect to complexity of crustal and lithosphere structure, however, CSS information alone may not adequately cover the region to construct a reliable Moho topography (Di Stefano *et al.* 2011). In principle, information obtained by other techniques, such as RF, LET and ambient noise tomography, could be added to improve coverage and reliability of the Moho topography. Different seismic methods, however, do not necessarily show the same characteristics in the data they produce, nor do they necessarily image the same structure at the same location with the same resolution (e.g. Holliger & Kissling 1992). The comparative use of seismic data and information derived by different seismic methods to construct Moho maps is, however, of great significance. Such models, by depicting the lateral continuity of differently imaged structures, are needed to crosscheck results from different seismic investigations and to use them as *a priori* information in inverse problems (e.g. Hrubcova & Geissler 2009).

In this study, we document a new methodology to quantitatively combine CSS and RF information to derive the Moho topography for the central Mediterranean area. The strength of CSS profiling is the qualitative identification of seismic phases and their quantitative interpretation as individual Moho reflectors and refractor elements at depth. In addition, to being a 2-D method requesting migration, the limitations of CSS methodology also regard the intrinsic bias

to locally sample higher velocity regions as well as the ambiguity when interpolating the relative sparse information in regions with few profiles, that is, central and southern Italy. RF studies best reveal relative depth variations of velocity interfaces such as Moho between nearby stations. RF are sensitive to first-order velocity discontinuities through phase conversions *P* to *S* and *S* to *P* (Langston 1979), see Fig. 2(a). Other intracrustal discontinuities may also be mapped, usually showing less prominent signals than the Moho. In addition, RF maps the average V_p/V_s ratio over whole or large parts of the crust, and, therefore, RF signals are excellent providers for body *S*-wave information, that is otherwise more difficult to obtain than *P* information.

Overall, RF studies draw detailed pictures of local Moho geometries, that have been shown (Lombardi *et al.* 2008) to be in good agreement with the more regional trends of the *a priori* established Moho map (Waldhauser *et al.* 1998). Recent studies provide a combination between results of these two methodologies (e.g. Hrubcova & Geissler 2009; Di Stefano *et al.* 2011) without introducing an uncertainty scheme for RF data analogous to that proposed by Waldhauser *et al.* (1998) for CSS data.

To allow a consistent and homogeneous derivation and combination of CSS and RF results, we introduce a new classification/weighting schemes based on uncertainty for RF data, specifically designed to match the criteria proposed in Waldhauser *et al.* (1998). In order to tune the RF information quality, we compare RF Moho depths and estimate uncertainties with high-quality CSS information and well-resolved LET-derived Moho (Diehl *et al.* 2009; Di Stefano *et al.* 2009). Subsequently, the Moho interface for the entire central Mediterranean region is calculated interpolating all CSS and RF data following the principle of simplicity described in Waldhauser *et al.* (1998).

2 METHODOLOGY TO DERIVE CSS AND RF INFO FOR 3-D MOHO TOPOGRAPHY

The derivation of a reference 3-D crustal model based on both RF and CSS data requires a comparative analysis of the strengths and limitations of these two methodologies to map Moho topography and an assessment of the quantitative uncertainties of information resulting from these methods. Reliability and precision of the CSS information depend on observed data quality, interpretation methods and orientation of 2-D profiles with respect to 3-D structure. A full explanation of the compilation procedure for CSS information is reported by Waldhauser *et al.* (1998). In the following, we just summarize fundamentals of the procedure.

2.1 CSS information and weighting scheme

In Waldhauser *et al.* (1998), the reliability and error assessment of the various collected CSS information over time is based on weighting schemes for refraction and reflection profiling that express the level of confidence for each individual seismic structure (Kissling 1993; Baumann 1994; Kissling *et al.* 1997). Along reflectors/refractors, information quality may vary due to different phase data quality, interpretation procedure and depending on type of profile. The weighting scheme proposed by Waldhauser *et al.* (1998) differs for wide-angle and near-vertical reflection surveys. Reflector elements derived from wide-angle profiles are weighted considering the quality and correlation of observed phases (w_c), profile orientation relative to the 3-D tectonic setting (w_o) and profile
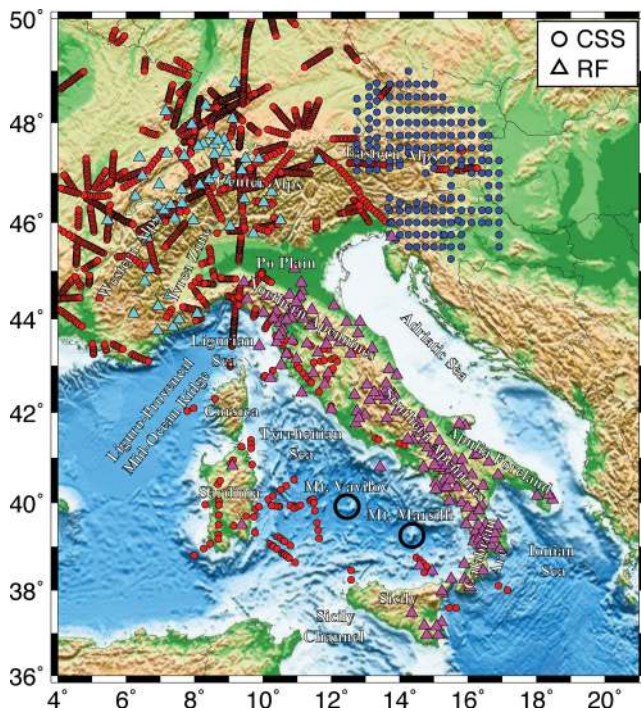
Figure 1. Schematic map of the central Mediterranean region including all available CSS and RF information in the area. Triangles in cyan and purple indicates the Piana Agostinetti & Amato (2009) and Lombardi *et al.* (2008) data set, respectively. Red circles indicates CSS information compiled by Di Stefano *et al.* (2011) and references therein following the weighting scheme propose by Waldhauser *et al.* (1998). Blue circles indicates CSS information compiled in this paper following the weighting scheme above for the profiles for the eastern Alps published in Behm (2006), Behm *et al.* (2007) and Brueckl *et al.* (2010). Black circles indicate the location of the Vavilov and Marsilli seamounts in the Tyrrhenian Sea.

type (i.e. whether the profile is reversed, unreversed or a fan) (w_t). Reflector elements derived from near-vertical profiles are weighted considering the quality of the reflectivity signature (w_{cr}), type of migration (i.e. source of velocity used for migration) (w_{mig}) and projection distance (w_{proj}, projection of subsections on to one reflection profile). A total weighting factor (w_{tot}) is obtained for each segment of the reflector, by multiplying the individual weights. The total weighting factors are then transformed into a depth error estimate by computing the corresponding first Fresnel volume (e.g. Kissling 1993). Considering an average frequency content of 6 Hz for Moho reflections from active sources and an average Alpine Moho depth of 40 km, and assuming optimal profile design and optimal data (w_{tot}), an optimal vertical resolution of ±3 km is derived (Waldhauser *et al.* 1998). Thus, the individual error estimates are calculated as the ratio between the minimal uncertainty (±3 km) and the individually determined w_{tot}. Along reflectors/refractors, weighting may vary due to different phase quality and depending on reversed or unreversed profile. In this study, we use the CSS information including their weights compiled by Di Stefano *et al.* (2011) and references therein (Fig. 1). We also collect information from the CSS experiments reported by Brueckl *et al.* (2010) for the eastern Alps. In addition to profile information, we extract well-resolved Moho depths from the Moho map published by Behm (2006) and Behm *et al.* (2007) based on PmP wide-angle reflections. In their overlapping parts, the Moho map by Behm *et al.* (2007) is in good agreement with the well-resolved LET-derived Moho from Diehl *et al.* (2009) for the eastern Alps. To all CSS

data, we apply the weighting scheme proposed by Waldhauser *et al.* (1998).

2.2 A weighting scheme for RF information

To complement CSS observations while maintaining the implicit consistency of the seismic data set, we derive RF Moho information following an analogue weighting scheme as for CSS info to assess individual uncertainties. In this paper, we use the RF data sets from Piana Agostinetti & Amato (2009) for the Italian peninsula and Lombardi *et al.* (2008) for the western Alpine region. We divide the RF data in different quality classes by defining some general criteria applicable to the radial component of the RF result.

The criteria regard the quality of the summary RF signal, that is, clearness of RF *P* onset relative to noise and shape of the signal, the certainty of Moho signal identification, and how representative this observed summary RF is with respect to the best possible observation at a station, that is, when it would be the sampled over all backazimuth (BAZ):

(i) the identification certainty of *Ps*–Moho phase;
(ii) the total azimuthal coverage;
(iii) the variation of the sharpness of the *Ps*–Moho phase along the BAZ;
(iv) the dipping Moho interface.

The separate evaluation by these criteria are necessary because the azimuthal coverage and the wave form of the RF represent independent and different data qualities that both affect the overall uncertainty of the interpreted Moho depth. The four criteria are chosen according to the estimated main sources of uncertainty of RF information (see Fig. 2). While in refraction seismics combined PmP and Pn phases provide unique information on Moho, in RF signal the Moho phase is usually the strongest of few possible. Points (ii) and (iv) are related to the horizontal resolution and point (iii) to the vertical resolution.

The resolution of RF Moho information (Fig. 2) primarily depends on the wavelength of the incoming *P* and the converted *S* phase interacting at the Moho. The presence of heterogeneities along the volume traversed by the rays as well as lateral variations of the Moho will affect the amplitude of the converted *Ps* phase. Furthermore, the sharpness or smoothness of Moho strongly affect the *Ps* phase and its multiples. In the case of a distinct velocity discontinuity at the Moho, the amplitude of the converted phases are strong, while in the case of a more smooth velocity transition they are weak. In presence of normal noise (Sheriff & Geldart 1995; Yilmaz 2001), the optimal vertical resolution of RF for the Moho interface is estimated as ±0.1 s in the arrival time of the *Ps* phase (e.g. Lombardi *et al.* 2008).

Analogue to the resolution estimates for CSS (Kissling *et al.* 1997), the horizontal resolution (Fig. 2b) of RF is assessed by the first Fresnel volume as the extension of the area sensitive to a given wave front. The horizontal resolution strongly depends on the azimuthal coverage (Fig. 2d) (ii), and the lateral variation of the Moho, such as a dipping Moho (Fig. 2b) (iv). Since the *Ps* wave, however, seems not to be significantly affected by moderately dipping Moho, for a dip ≤15° Lombardi *et al.* (2008) estimate a maximum effect of less than ±0.1 s, the azimuthal coverage becomes the most important source of uncertainty for horizontal resolution: the better the azimuthal coverage the more precise the Moho discontinuity is resolved. In fact, incoming *Ps* waves
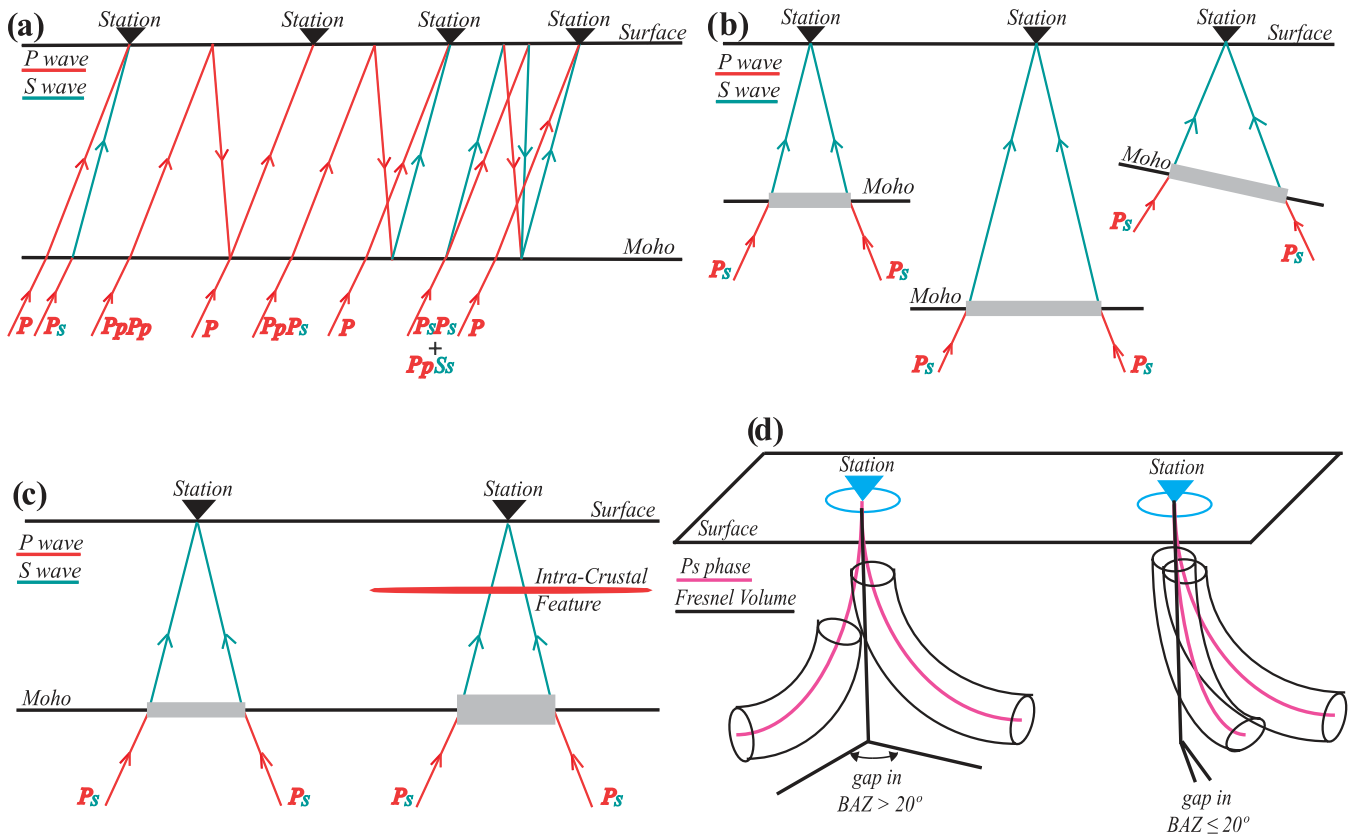
Figure 2. (a) Sketch diagram of an incident *P* phase and transmitted, reflected *P* and converted *S* for a simple one layer over half-space model. (b) Horizontal resolution (in grey) for different Moho depth and in case of dipping Moho. (c) Vertical resolution (in grey) in presence (right) or not (left) of heterogeneities in the volume. (d) Fresnel volume for ray coming from different backazimuth. On the left the Fresnel volumes are further away each other (backazimuth gap $\geq 20°$), thus there is no continuity in the RF azimuthal coverage. On the right, the Fresnel volumes overlap (backazimuth gap $<20°$), thus there is continuity in the RF azimuthal coverage.

arriving from a wide range of BAZ will resolve a subhorizontal Moho very well and they may even document a uniform dip of the interface, while data from only a narrow range of BAZ may not even resolve a flat Moho well. Therefore, the azimuthal coverage must be as large as possible, otherwise the estimated Moho depth will be biased by local crustal structure and scattering. Finally, the horizontal resolutions of a teleseismic RF for a first-order discontinuity interface, for example, Moho, depends on the depth of the interface [e.g. Lombardi *et al.* (2008)]. In general, lower horizontal uncertainties are commonly related to shallower Moho; while higher uncertainties are related to deeper Moho interfaces (Fig. 2b). In presence of normal noise (Sheriff & Geldart 1995; Yilmaz 2001), the horizontal resolution of RF for the Moho interface range from ~ 20 to ~ 30 km.

2.2.1 Identification of Ps–Moho phase

The first step is the correct identification of the *Ps* phase (e.g. Mele & Sandvol 2003). *Ps* conversions are best observed on the radial component of the RF. The *Ps*–Moho phase is generally clearly visible as the highest amplitude peak after the direct *P* arrival. In tectonically active regions as the Alps or the Apennines, occasionally there may be more than one positive high-amplitude peak sampled by RF near the plate boundaries. Positive-polarity *Ps* pulses indicate downward increase of velocity. In fact, the Moho discontinuity separates the high upper-mantle velocities ($V_p \sim 8.1$ km s^{-1}) from lower crustal

velocities ($V_p \sim 6.5$ km s^{-1}). An example of a picked *Ps* phase is shown in Fig. 3.

2.2.2 Azimuthal coverage

In the second step, we consider the BAZ coverage in the RF data (see Fig. 3), relative to $360°$ for subhorizontal Moho, and to both $180°$ sectors in the case of a clearly dipping Moho. We accept as continuous BAZ coverage if the Fresnel volumes of two neighbouring individual rays laterally overlap, see Fig. 2(d). To calculate the total BAZ coverage we consider the following points with regards to the lateral wave sensitivity (Fig. 2d and Fig. 3):

(i) in case between two resulting signals there is a gap $<20°$ with no significant variation in the signal, the gap will not be considered. In fact, for these gaps, the Fresnel volumes of each incoming 1 Hz teleseismic wave will largely overlap each other, see Fig. 2(d).

(ii) in case between two resulting signals there is a gap of $10° \leq$ gap $\leq 20°$ and the variation in the signals on either side of the gap is significant, the gap will be considered.

(iii) in case between two resulting signals there is a gap $>20°$, the gap will be considered.

In cases of shallower Moho (in the range 15–30 km) when the number of RF data is low and widely separated in BAZ, and the total azimuthal coverage is less than $180°$, we introduce a $20°$ bonus to add to the total BAZ coverage.
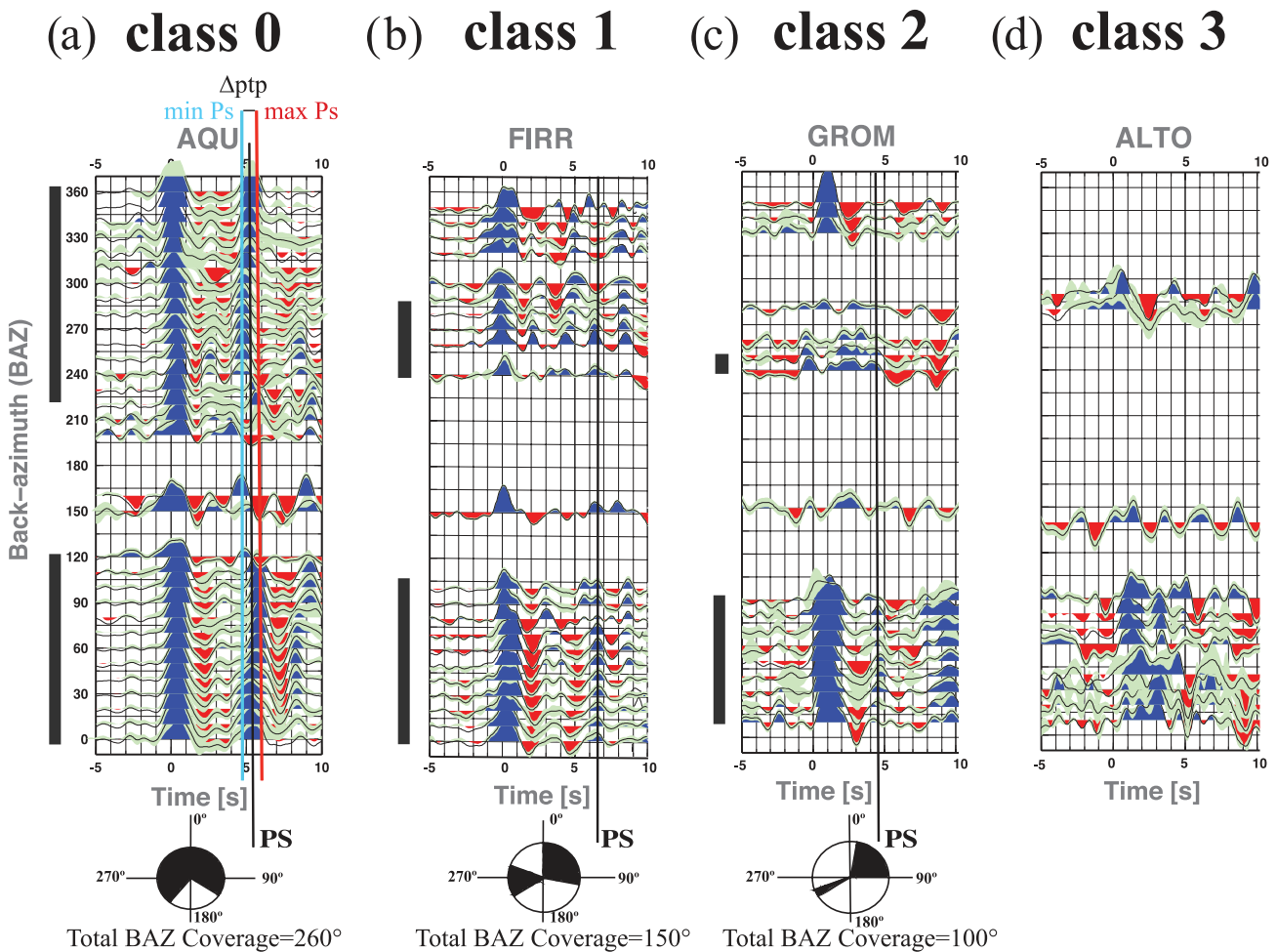
Figure 3. Criteria and classification for the RF data. The *Ps* phase is highlighted by a black line. The backazimuth coverage is highlighted with black rectangular shapes and circles, which are located behind the RF signal. The Moho depth is calculated using a $V_p = 6.5 \text{ km s}^{-1}$ and a $V_p/V_s = 1.725 \text{ km s}^{-1}$. (a) Class 0. The station AQU of the Italian Seismic Network. The blue line is the minimum pick *P–Ps* time (at 4.5 s) measure along the BAZ (a total of 260°) and the red is the maximum (at 5.5 s). The difference is the Δt_{ptp}, in this case 1 s. The Δt_w is not highlighted here. The estimated Moho depth is ∼43 km. (b) Class 1. The station FIRR of the Italian Seismic Network. General reduction of the backazimuth coverage and less clear identification of the *Ps* phase with respect to (a). The *Ps* phase is more or less identified between 6.0 and 6.2 s (Δt pick to pick = 0.2 s) along a total of 150° BAZ. The estimated Moho depth is ∼52 km. (c) Class 2. The station GROM of the Italian Seismic Network. General reduction of the backazimuth coverage and less clear identification of the *Ps* phase with respect to (b). The *Ps* phase is clearly visible between 4 and 4.5 s (Δt pick to pick = 0.5 s) along a total of 100° BAZ. The estimated Moho depth is ∼37 km. (d) Class 3. The station ALTO of the Italian Seismic Network. Not enough backazimuth coverage and no identification of the *Ps* phase.

2.2.3 Sharpness of the Ps–Moho phase

The third step regards the variation of the sharpness of the *Ps*–Moho phase along the BAZ. In this context we take into account both amplitude and time variations of RF data in relation to BAZ. To consider this variability we include the difference in time between the peak of the earliest Moho arrival and the peak of the latest Moho arrival for all BAZ, see Fig. 3(a). In this way, we can analyse the quality of the average RF Moho depth derived from our RF data in presence of local noise and heterogeneities in the volume beneath the station. Furthermore, this time difference is a rough measure of the vertical resolution of the Moho interface including possible effects of minor variations in the dip of the Moho.

2.2.4 Dipping Moho interfaces

In areas of dense RF coverage, an additional step in the classification of RF information could be the quantification of Moho dip and related horizontal resolution for cases where a dipping Moho can

clearly be identified. In presence of Moho dip, the RF information can be classified only in classes where the dip is accepted (Table 1). For the data set at hand, however, we do not have enough information to *a priori* estimate of dip of converted phases based on single station data alone. We decided not to consider this step in our classification. The main reasons are:

(i) effects of moderately dipping Moho on *Ps* phase are minor relative to other uncertainties. In fact, as discussed in Lombardi *et al.* (2008), for a $10° \leq \text{dip} \leq 15°$ one observes a relative delay time for different azimuth of less than 0.1 s for the *Ps* phase;

(ii) the combination of converted and multiple phases provide commonly not sufficient information to understand if the Moho is dipping or not as discussed in Peng & Humphreys (1997), Savage (1998), Lombardi *et al.* (2008).

(iii) the lack of data. In fact, in Europe the vast majority of teleseismic waves come from 240°–120° BAZ, while only about 5 per cent of all useful events are covering the rest of the BAZ circle. For example, in case of the Alps where the European Moho

Table 1. Classification of the RF information uncertainty. For the special classification, class 4 and class 2M, see the text. Note that a low-pass filter of 1 Hz has been applied to the seismograms for the calculation of the RF used in both Lombardi *et al.* (2008) and Piana Agostinetti & Amato (2009).

	Identification of *Ps*–Moho phase	Azimuthal coverage	Variation of the sharpness of *Ps*–Moho phase	Moho dip	Uncertainty
Class 0	Clear identification	BAZ $\geq 180°$	Time width $\leq \pm 0.5$ s Peak to peak time $\leq \pm 0.5$ s	No dip accepted	± 3 Km
Class 1	More or less clear identification	$150° \leq$ BAZ $\leq 180°$	Time width $\leq \pm 0.6$ s Peak to peak time $\leq \pm 0.6$ s	Dip accepted	± 6 Km
Class 2	More or less clear identification	$90° \leq$ BAZ $\leq 150°$	Time width $\leq \pm 0.8$ s Peak to peak time $\leq \pm 0.8$ s	Dip accepted	± 10 Km
Class 3 (rejected stations)	Poorly identifiable	BAZ $\leq 90°$			
Class 4	Special classification when both intracrustal feature and Moho interfaces are detected (see text)				
Class 2M	Special classification when two overlapped Moho interfaces are detected (see text)				

is generally dipping in southward directions, it will be impossible to quantify this Moho dip by RF due to lack of data from Africa.

2.2.5 Moho depth estimation

The crustal thickness estimation (*H*) is related for RF to the time delay of the incoming *Ps* phase with respect to the first arrival *P*, to the V_p/V_s ratio (*k*) and to the ray parameter *p* as follows (Zhu & Kanamori 2000):

$$H = \frac{t_{Ps}}{\sqrt{\frac{k^2}{V_p^2} - p^2} - \sqrt{\frac{1}{V_p^2} - p^2}}. \tag{1}$$

We calculate the Moho depth estimating *p* based on the IASP91 model and using a constant crustal V_p/V_s ratio of 1.725 and an average V_p velocity of 6.5 km s^{-1}. We use an average V_p in order to be consistent within the entire study region, since only in a few locations coinciding CSS and RF data are available.

2.2.6 Classification of the RF data and related uncertainty in Moho depth

Based on the general criteria described in the previous section, we define Moho uncertainty classes for RF information. We propose four general classes, from 0 (top) to 3 (not to be used), and two special (4 and 2M) for additional information. For example, a RF information in the top quality class (class 0) has a high-quality summary RF signal, that is, a clear identification of *Ps*-Moho signal, with a sharpness (half-wave length) of the same phase ≤ 0.5 s, and a very high BAZ coverage ($\geq 180°$) with fair to good individual Moho signals. The general classification is summarized in Table 1 and examples for each class are shown in Fig. 3.

The two special classes include all stations with Moho signals classified as described above that show the presence of specify additional interfaces. In class 2M, we include the stations showing a clear presence of two Mohos. In RF results it is possible to identify, in some cases, two clearly separated amplitude maxima comprising a 'dual-peak' *Ps* phases. In such a cases we check for a possible double Moho interface beneath the station (Fig. 4). The identification of two maximum peak amplitudes is, however, not sufficient to define two Moho above each other. In fact, artefacts or noise in the signal could produce fictitious maximum peak amplitude with the consequence of an incorrect interpretation of the RF data. To avoid this problem, first of all, we need to compare the location of

the station and the tectonic map of the region to know if a double Moho interface is possibly present due to plate boundary tectonics. Secondly, the presence of anisotropy between the upper and the lower Moho interface has to be visible in the transverse component of the RF result (Fig. 4). Anisotropy in RF transverse component is identified as an inversion of the signal along BAZ between the two probable *Ps* –Moho phases (Fig. 4). In recent studies, for example, Fry *et al.* (2010) and Bianchi *et al.* (2010b), it could be shown that anisotropy between the two Mohos is present due to the layer of peridotitic (upper mantle) material below the upper Moho resting atop the lower crustal material above the second Moho.

In special class 4, we include all stations showing a clear presence of an intracrustal interface. In some cases, beside the *Ps*–Moho phase, it is possible to identify another *Ps* phase—usually also of positive amplitude—that is the converted *P* to *S* wave of an intracrustal interface. These phases, which we call *P-intra* (Fig. 4) may be very difficult to spot in noisy data. The main differences between an RF showing two Mohos and an RF showing an intracrustal and a Moho interface is that, under normal circumstances, in the latter the peak of amplitude of the intracrustal feature is clearly lower than the peak of amplitude generated by the Moho interface and that there is no typical anisotropy effect present on the transverse component (e.g. Bianchi *et al.* 2010b). For stations included in class 4, each interface (Moho and intracrustal) at first is classified individually. However, due to the presence of an intracrustal feature that could possibly interfere with the *Ps*–Moho phase, and thus hamper correlation and timing, the class of the Moho interface is downgraded by one class. This is valid for classes 0 and 1, but it's not applicable to class 2, since otherwise the station will be excluded.

For each of the four general classes (from 0 to 3), we estimate a general uncertainty value in Moho depth. We base our estimations on the discussion of the vertical resolution of RF (see Section 2.2). From the sharpness of the *Ps* phase onset, that is, the timing uncertainty, we calculate the Moho uncertainties using the Zhu & Kanamori (2000) equation (see eq. 1). We then estimate the mean of the Moho uncertainties within each defined quality class taking into account Fresnel volume and sampling geometries. For example, we estimate the vertical resolution for top-quality RF (class 0) with strong *Ps* phase amplitude, and with excellent BAZ coverage of more than $180°$ for the Moho discontinuity to be about ± 3 km. This value correlates well with the top-quality CSS vertical resolution (Waldhauser *et al.* 1998). For RF of quality class 1 and 2 the Moho depth uncertainties are estimated as ± 6 and ± 10 km, respectively.
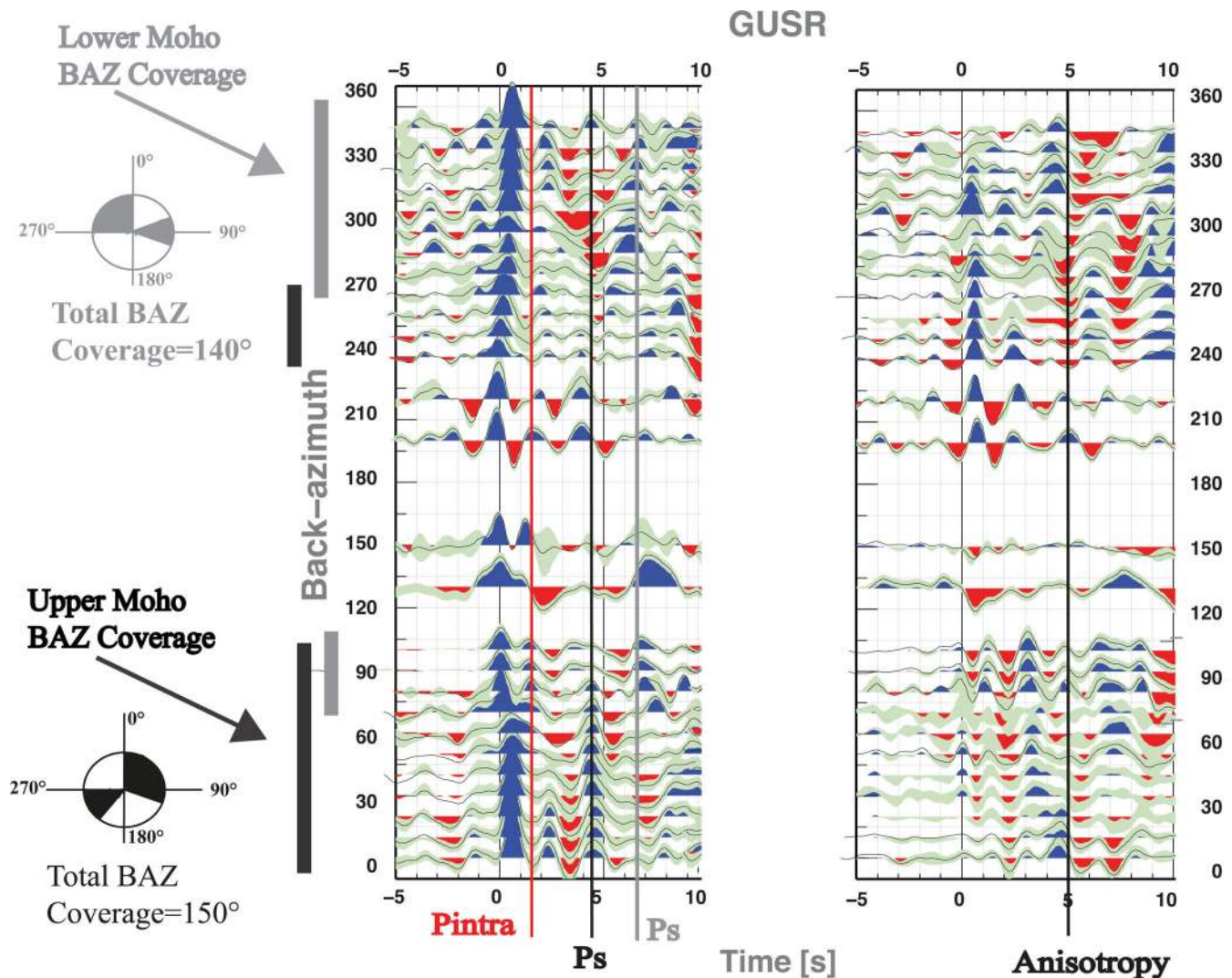
Figure 4. Example of class 4 and class 2M. The backazimuth coverage is highlighted with rectangular shapes and circles. The two Mohos and the intracrustal feature depths are calculated using a $V_p = 6.5\,\mathrm{km\,s^{-1}}$ and a $V_p/V_s = 1.725\,\mathrm{km\,s^{-1}}$. On the left the radial component and on the right the transversal component for the station GUSR of the Italian Seismic Network. On the radial component, the red line pick the *P*-intra phase, that is the converted *P* wave from an intracrustal feature. It is visible between 1.5 and 2.5 s along 180° BAZ. The estimated depth is ∼16 km. The black and grey lines show the peak of the Mohos. The first maximum peak amplitude (black line) is visible between 3.5 and 4.5 s along 150° BAZ, while the second one (grey line) is visible between 6.5 and 7.5 s along 140° BAZ. The estimated depth is ∼34 and ∼56 km for the upper and the lower Moho, respectively. On the transverse component, the black line indicates where the inversion of the signal is present highlighting the anisotropy. There is a clear inversion from a negative, within 0°–60° and 300°–30° BAZ, to a positive, within 80°–100°, 240°–280° BAZ, sign of the signal around 5.5 s.

2.2.7 Summary of RF data classification

In this study, we use the RF data sets from Piana Agostinetti & Amato (2009) for the Italian peninsula and Lombardi *et al.* (2008) for the western Alpine region (Table S1). We classify the stations belonging to Piana Agostinetti & Amato (2009) data set as shown in Fig. 5(a). In case of Lombardi *et al.* (2008) we have only a general knowledge on BAZ coverage, but individual RF signals are not available to assess classification. Hence, we classify the RF information based on the identification of the multiple phases in Lombardi *et al.* (2008). Based on summary RF signals, in a first step we classify all stations with a correct identification of the multiple phases, identifiable only in the presence of a flat Moho, in class 0, while in cases where only the *Ps* phase is identified, the RF is estimated as class 1. In a second step, we downgrade the classification by one class, since we have no detailed information

on how the observed summary RF are sampled over all BAZ. In this study only the high-quality RF (class 0 and class 1) are used (Fig. 5b). Furthermore, RF information that belong to class 2M will be taken into account as well.

2.2.8 Tuning RF uncertainty estimation with CSS and LET data

The qualitative uncertainty for RF data are defined based on the classification scheme proposed above and corresponding quantitative uncertainty estimates are based on theoretical consideration. When compiling a Moho map from RF and CSS data combined, quantitative error estimates for both data sets must match. Considering only high-quality RF data (class 0, class 1 and class 2M) we compare them with the CSS classification by Waldhauser *et al.* (1998) and, in particular, with corresponding CSS data in the study
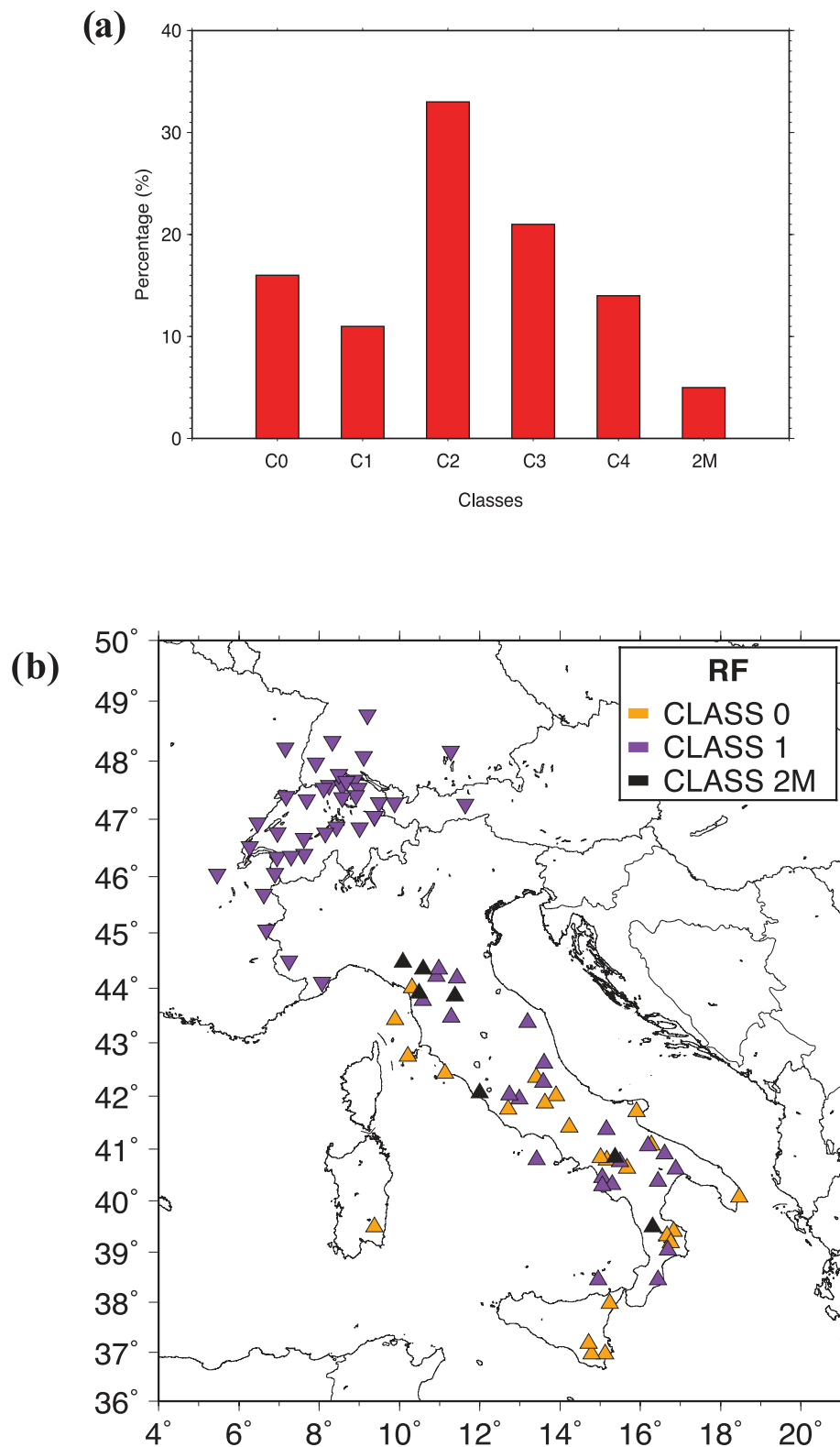
(a)

(b)

Figure 5. (a) Percentage of RF for each class for the Piana Agostinetti & Amato (2009) database. (b) The RF in high-quality classes, class 0 and class 1, and in class 2M use in this study. The triangles and inverse triangles indicate the Piana Agostinetti & Amato (2009) and Lombardi *et al.* (2008) data set, respectively.

region reported by Waldhauser *et al.* (2002), Di Stefano (2005) and Di Stefano *et al.* (2011). In addition, we also compare our RF-derived local Moho information with recently published high-resolution LET information (Diehl *et al.* 2009; Di Stefano *et al.* 2009).

In the first step we compare CSS-derived Moho depths and uncertainties with the RF-derived Moho depths and uncertainties where both data are available for same location. We find a very good correlation between the CSS and RF information in all cases (Fig. 6). In general, the quality of the CSS in the region, however, is only fair
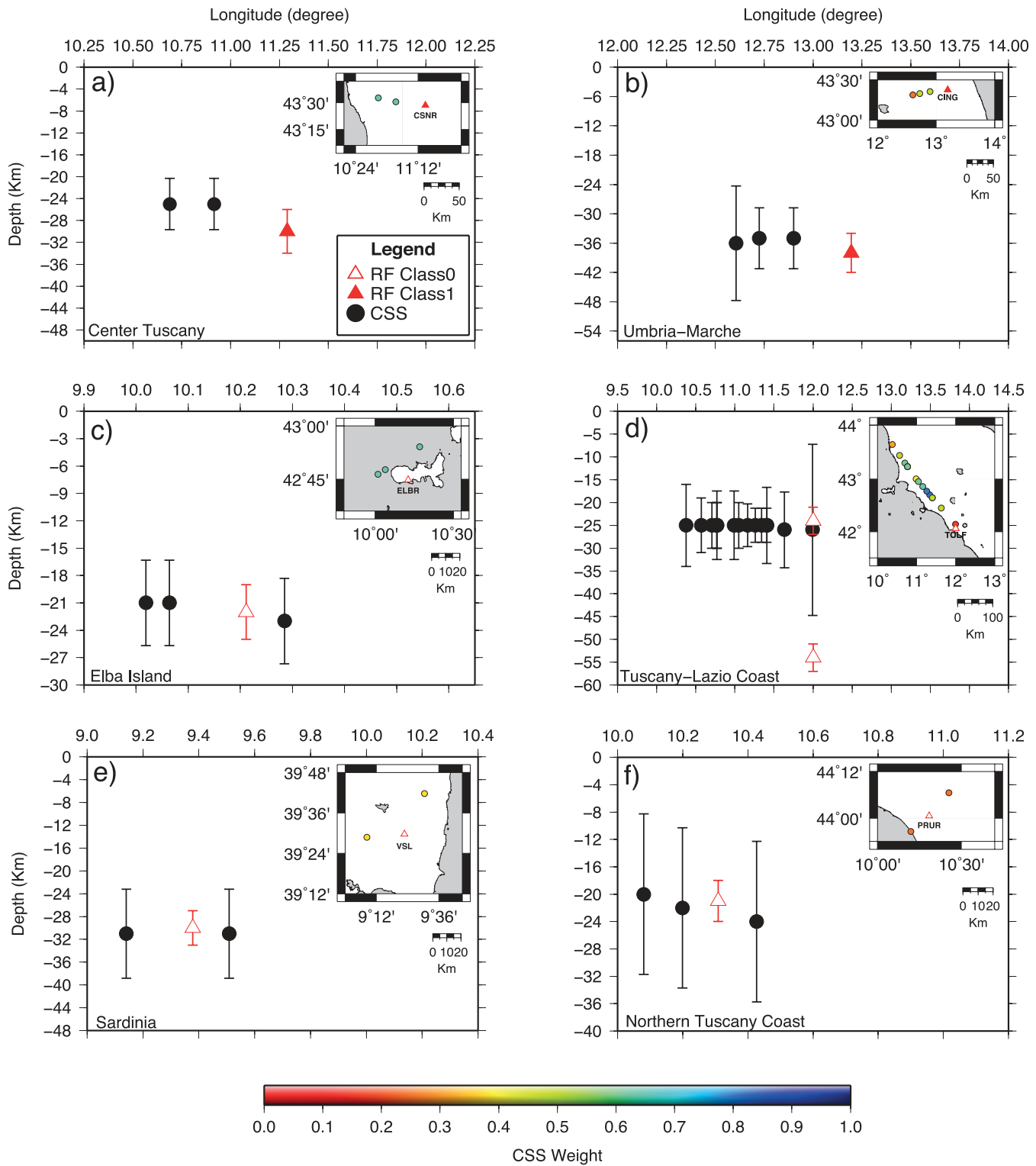
Figure 6. Comparison between RF and CSS data including uncertainty estimates. In black the CSS data including uncertainty estimation based on the weighting scheme. Note that in this example CSS data of rather poor quality are compared with RF data of rather good quality. Red triangles, RF information including uncertainty estimates. The empty triangle highlight class 0 RF. The full triangle highlight class 1 RF. The colored circles in the maps indicate the weight of each CSS information.

to poor, and certainly not adequate to resolve Moho in subduction zones. Moreover, when considering the combination of the rather poor quality with the rather sparse CSS information in the region, we conclude the CSS data are insufficient to tune the RF uncertainty estimation.

Hence, in a second step we compare the RF information with high-quality LET results. Since there are no LET studies for the entire study region, we use the LET from Diehl *et al.* (2009) for the western Alpine region and the northern Apennines and Di Stefano *et al.* (2009) for the northern Apennines and Central and

southern Italy. The comparison between the two models in the overlapping region (Figs 7a and b) is assessed in order to have a common and reliable information on the LET-derived Moho for all Italian region. In spite of different parametrization, damping and database, a comparison of the tomography-derived Moho and average crustal velocity in the northern Apennines region, based on the methodology proposed by Wagner *et al.* (2012), reveals a good general agreement between the results by Diehl *et al.* (2009) and Di Stefano *et al.* (2009). In Diehl *et al.* (2009) just a small region around the suture zone between the Tyrrhenic and the Adriatic Moho is well resolved, while in Di Stefano *et al.* (2009) no quantitative information of the resolution is available, but qualitative estimates document all of Italian peninsula being well resolved (Figs 7a and b). The well-resolved tomography-derived Moho topography in Diehl *et al.* (2009) for Adria and for Tyrrhenian (approximately represented by $V_p = 7.25\,\mathrm{km\,s^{-1}}$ and $V_p \sim 7.0\,\mathrm{km\,s^{-1}}$, respectively, see Wagner *et al.* 2012) fit particularly well with the tomography-derived Moho in Di Stefano *et al.* (2009) (Figs 7a and b).

We observe a maximum difference of 4 km in the northern Apennines for the two LET studies. Therefore, a conservative uncertainty estimate for the LET-derived Moho depth is ±3 km, in accordance with the estimate by Wagner *et al.* (2012) for top-quality LET information and in good correlation with the minimum relative uncertainty estimation for the RF information (±3 km). We use these values in order to tune the high-quality RF uncertainty estimation in the central and southern part of the Italian region, where only qualitative resolution information is available by Di Stefano *et al.* (2009). Then, we compare the well-resolved LET Moho estimation from Diehl *et al.* (2009) with the RF information in some cross-sections in the northern Apennines (Fig. 7b). For each RF, we first analyse the data, combining the maximum *Ps* peak amplitude and its BAZ to assign the information to the correct Moho interface (Fig. 7d). In fact, the combination of the two provide the information from what direction the seismic energy is coming and, hence, which of the two Mohos at the plate boundary in each case is converting (RF) the incoming wave.

Since RF provides 1-D information in 3-D environment, they are subjected to possible migration. Small scale 3-D migration is constrained by the BAZ-related resolution of the RF, and thus included in our uncertainty estimates. In those cases, however, where we see doubled Moho converters in RF near plate boundaries and in regions well-resolved by LET (see above), we are able to correlate them easily by more pronounced, but realistic 3-D migration to the two Moho surfaces Liguria/Tyrrhenia and Adria across the suture zone (e.g. the red arrow in Fig. 7b).

Once each RF information is assigned to the correct Moho interface by 3-D migration across the Moho offset (Fig. 7b), we compare their depth with the well-resolved LET-derived Moho (Diehl *et al.* 2009). In general, we find an excellent correlation for the Adriatic Moho between the two methodologies. For the Tyrrhenian Moho, the RF results are systematically shallower than the LET results, but still within estimated uncertainties. The CSS information though sparse and distant from the RF data shows similar results as the RF information for the Tyrrhenian Moho, see, for example, the dashed red line in Fig. 7(b). From previous studies (e.g. Margheriti *et al.* 2006; Piana Agostinetti & Amato 2009) the Tyrrhenian Moho is estimated at ∼25 km depth off-shore, between Corsica and northern Italy, slightly dipping NE onshore in Italy. Overall, we note a very good agreement between all seismic data.

2.2.9 RF discretization for interpolation

RF Moho data are products of a 1-D method, thus they describe the depth of a velocity discontinuity (such as the Moho) within a certain region, defined by a circular area sample by the incoming seismic rays (horizontal resolution), at a given depth (Fig. 8a). The size of this region is defined by the Fresnel volume of the *Ps* and the multiples waves registered at the station. Thus, it depends on the depth of the discontinuity as well as on complexity of the velocity structure beneath the station. The deeper the Moho the larger is the region sampled by the RF (Fig. 8a). Based on this assumption and the classification/weighting factors of each RF information, we define a square region covered by the RF information at the Moho depth. The size of the square region is defined by the horizontal profile length resolved by the RF. Then, the square region is discretized in points base on the weighting factors, see Figs 8(b)–(d).

3 MODELLING 3-D CRUSTAL–MANTLE BOUNDARY IN ITALY

The geodynamic setting of the greater Alpine-Mediterranean region is the result of the NNW–SSE convergence between Africa and Eurasia plates and accommodated by a mosaic of microplates during subduction and collision in the Alpine and Apennines belts (Handy *et al.* 2010), Fig. 1. The puzzle of microplates move and deform partly independently from the overall large plate convergence (Reilinger *et al.* 2006). The structural setting of the central Mediterranean carries the characteristic processes, such as subduction, continental collision, rifting, slab rollback and backarc spreading that over long periods were geodynamically active (Dercourt *et al.* 1986; Malinverno & Ryan 1986; Faccenna *et al.* 2001, 2002; Faccenna & Becker 2010). These processes involve the main plates of Eurasia, Adria and Africa, separated by the Mesozoic Tethys and the Permo–Triassic Neotethys oceans.

We may put the beginning of the Alpine convergence around 80–90 Ma (e.g. Handy *et al.* 2010). In this period the Mesozoic Alpine Tethys began to close due to the convergence of the European and African plates (e.g. Capitanio & Goes 2006). The subduction of the Alpine Tethys ocean began at 85 Ma (e.g. Babist *et al.* 2006), followed by continental collision of Adria and Europe around 40 Ma (Handy *et al.* 2010). The convergence of the European and African plates continues until today, leading to the formation of the Alpine chain.

The Apennines formed more recently starting in the early Oligocene 35 Ma ago due to the subduction of the southwesternmost part of the Neotethys ocean, and slab retreat leading to asymmetric opening of the Tyrrhenian sea (12 Ma to present) (e.g. Faccenna *et al.* 2002). The latter was followed by the formation of localized spreading centres (4 Ma, Vavilov basin, 2 Ma, Marsili basin) with drifting and arching of the Calabria block (Faccenna *et al.* 2001), Fig. 1. Presently the central Mediterranean region has evolved into a jigsaw puzzle of irregular plates and fragmented slabs.

Even if the Mediterranean region is formed by a puzzle of irregular plates, at least three major crustal blocks and, hence, Moho discontinuities can be identified: the Adriatic-Ionian–African Moho (Adria), the European Moho (Europa) and the Ligurian–Sardinia–Corsica–Tyrrhenian Moho (Tyrrhenia). The Adriatic, African and Ionian plates can be considered as different parts of the same plate since there is no strong evidence for a seismically active plate margin between the southern part of Adria and the Ionian lithosphere (Chiarabba *et al.* 2005). We consider the Sardinia–Corsica block to be part of the Tyrrhenian, knowing that before its counter-clockwise
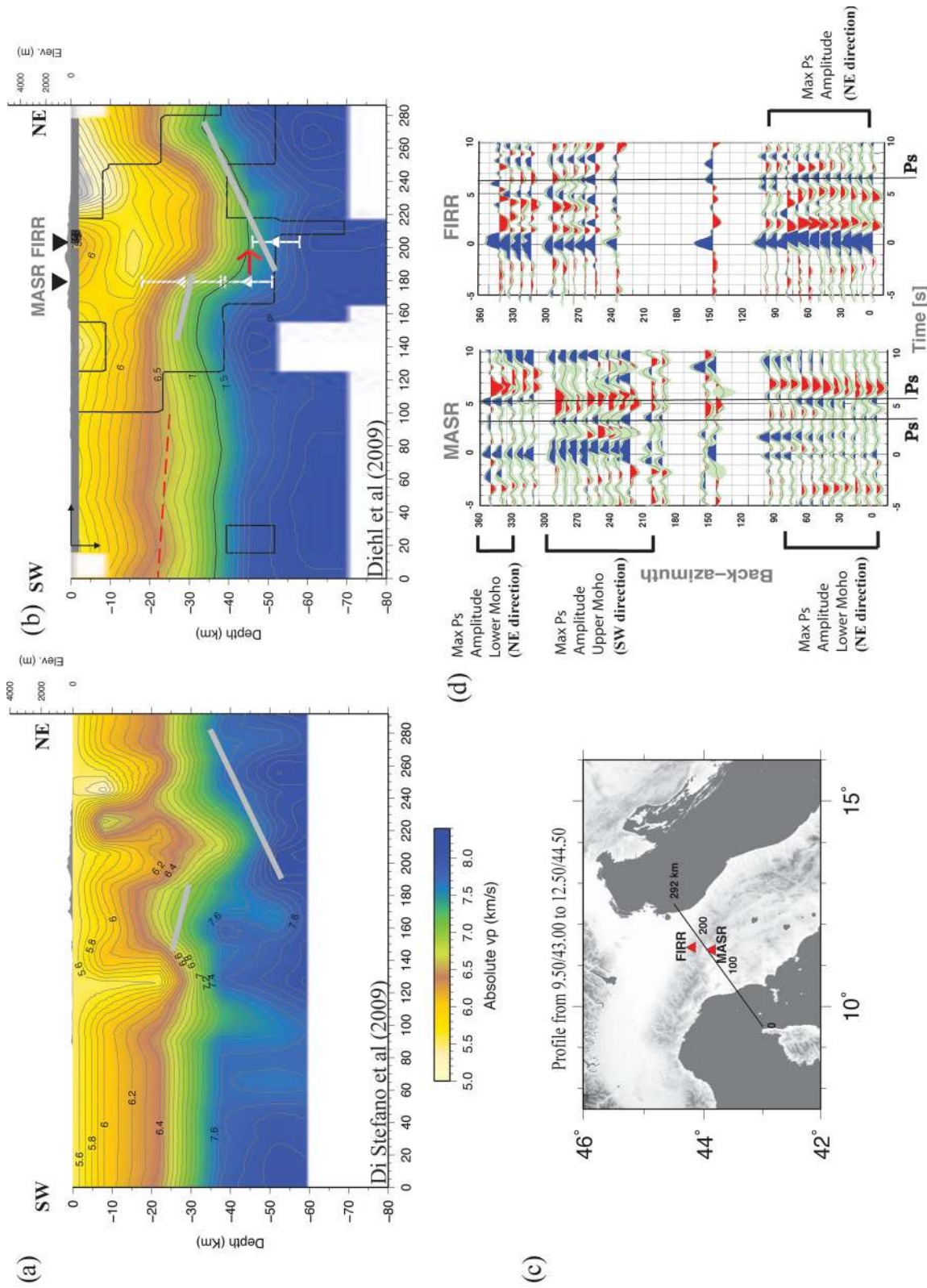
Figure 7. (a) LET cross-section from Di Stefano *et al.* (2009). In grey the LET-Moho derive from Diehl *et al.* (2009). (b) LET cross-section from Diehl *et al.* (2009). In grey the LET-Moho derive from Diehl *et al.* (2009). In white the RF data along the profile and their uncertainty estimation from this study. Red dashed line is the interpolation of CSS points along the crossection. The red arrow indicates the direction of the possible RF 3-D migration for the deeper Moho beneath MASR. For example, the lower Moho picked at station MASR can be migrated at least 10 km NE direction based on its horizontal resolution, a perfect fit is achieved. (c) Location of cross-section across northern Apennines. The red triangles indicates the station in which the RF are calculated. (d) RFs calculate for station MASR and FIRR with respect to backazimuth. For station FIRR, the maximum amplitude of the *Ps* phase is visible in the range between 0° and 80°. Thus, the Moho refracting the incoming ray is the Adriatic one. In case of the station MASR, the upper Moho has maximum amplitude of the *Ps* phase in the range between 200° and 300°. Thus, the incoming ray path is refracting by the Tyrrhenian Moho. The lower Moho for MASR has maximum amplitude of the *Ps* phase in the range between 340° and 70°. Thus, the incoming ray path is refracting by the Adriatic Moho.
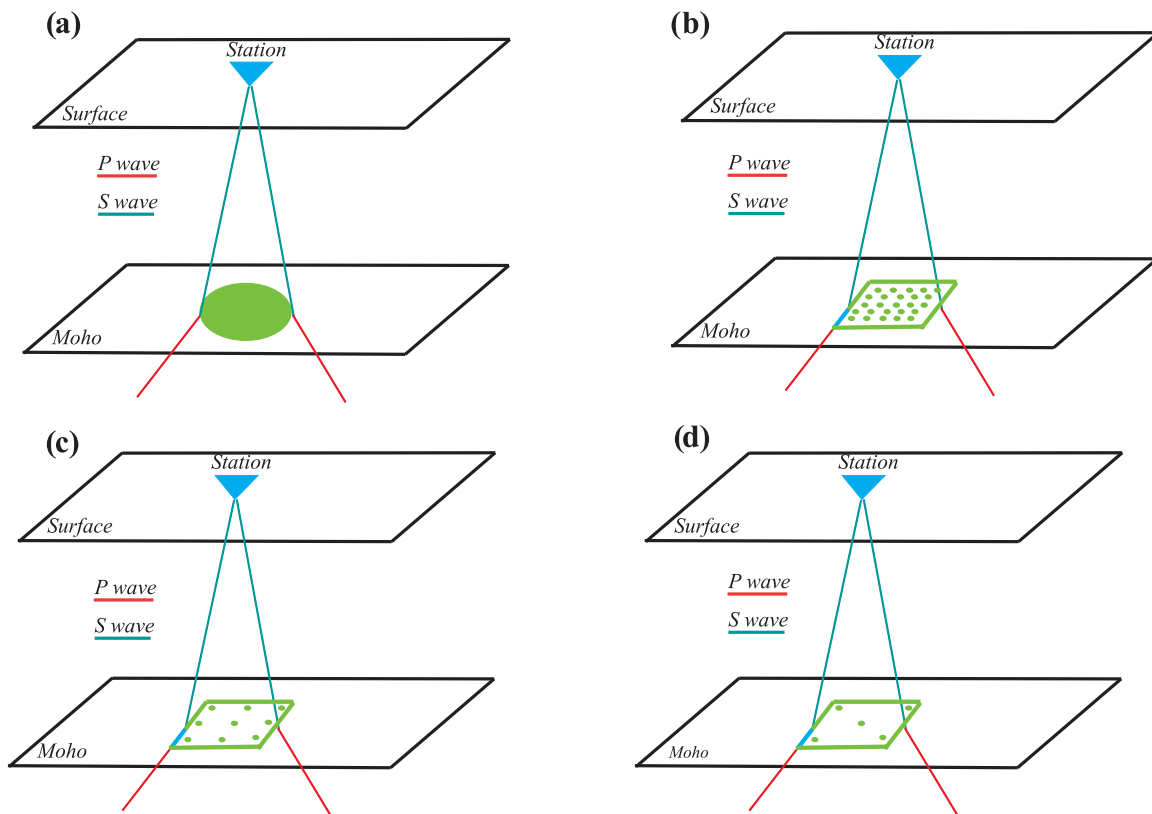
Figure 8. (a) Region in which the velocity discontinuity at depth is visible by an RF. (b) Discretization in 25 points of the region resolves by a top quality RF. (c) Discretization in nine points of the region resolves by a RF in class 1. (d) Discretization in five points of the region resolves by a RF in class 2.

rotation it was part of the Eurasian Plate (e.g. Faccenna *et al.* 2002). Tyrrhenia is characterized by different kind of lithospheres (thinned continental to the north and oceanic to the south) in different stages of evolution from north to south and from the west to the east of the Tyrrhenian Sea (Faccenna *et al.* 2001).

3.1 Interpolation Method

The interpolation method has originally been developed to generate a detailed 3-D velocity model of the crust by integrating Moho depths and velocity information retrieved from CSS 2-D profiles by weighting each data point according to its quality. A full explanation of the interpolation technique for Moho surfaces is reported in Waldhauser *et al.* (1998). We summarize fundamentals of the basic method and its implementation to complement the CSS data with the high-quality RF information.

The Moho interface is generated following the principle of simplicity: we search for the smoothest (simplest) Moho interface that fits all available information within their uncertainties (Kissling 1993). Thus, we define the simplicity of a seismic interface by the degree of continuity and the degree of surface roughness of this interface. The lateral continuity of an interface is achieved by interpolation between observed data. Regions characterized by complex tectonic setting, such as the Italian peninsula, usually exhibit large variability of Moho offsets. Such variability has to be taken into account in the interpolation process. Small offsets do not force the interpolation surface to lay outside the data error boundaries and thus they may be modelled at the cost of a small increase of roughness value. On the other hand, large offsets, such as major lithosphere plate boundaries (e.g. Adria–Tyrrhenia), can not be modelled with

a single Moho surface due to the abrupt change in depth larger than the estimated depth errors for two consecutive data points at the boundary. Hence, their modelling comes at the cost of increasing the overall complexity by allowing laterally discontinuous Moho interfaces.

To account for documented Moho offsets along plate boundaries, three main surfaces are used to fit the data and thus each Moho surface is related to a specific crustal block based on *a priori* information (Fig. 9). In the Alpine region we use the interfaces described in Wagner *et al.* (2012) based on an extensive analysis of the LET (Diehl *et al.* 2009), CSS (Waldhauser *et al.* 1998) and teleseismic tomography information in the region (Lippitsch *et al.* 2003). In the rest of the Italian peninsula, starting from the polygons defined in Di Stefano *et al.* (2011), we redefine the geometry of the boundary by careful analysis of LET information (Di Stefano *et al.* 2009) and of the high-quality RF data (e.g. Bianchi *et al.* 2010b) and ambient noise tomography studies (Verbeke *et al.* 2012), see Fig. 9. In addition to the definition of polygonal interface boundaries, supporting points for each interface are needed to prevent numeric instabilities when interpolating in poorly sampled region (Waldhauser 1996). Supporting points are located outside the real surface and are positioned in order to avoid overswing effects in the Moho surface by the interpolation process. Their Moho depth is always chosen to be equal to the nearest real point in the surface. While supporting points denote estimated depths of the Moho discontinuity, they are only used to insure that the Moho surface is smooth where it is otherwise poorly constrained. In this case, the corresponding crustal and top mantle velocity values remain as defined by the initial 1-D reference model. In the Tyrrhenian basin, we include supporting points as defined by Di Stefano *et al.* (2011) extrapolating from well-sampled regions for the different lithosphere types and for
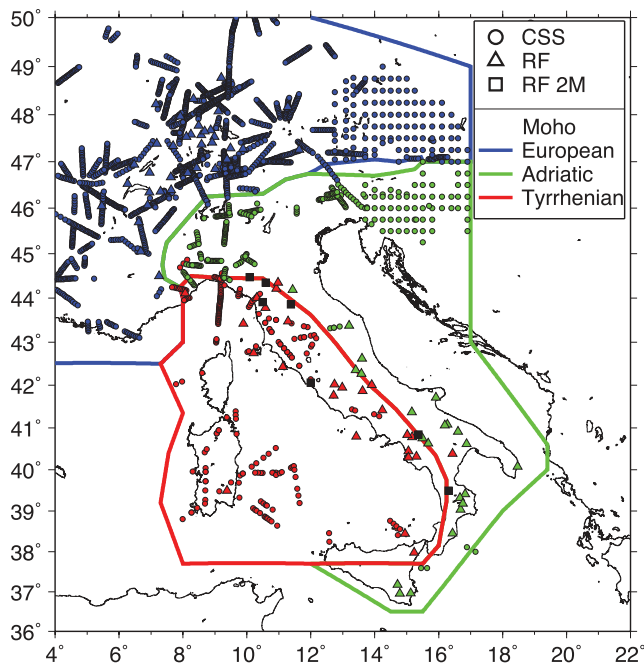
Figure 9. Geometry of the polygons defining the limits of the three Moho surfaces and RF high-quality and class 2M informations and CSS segments use to generate the Moho map.

tectonic settings. These points help the interpolation procedure to create a more realistic variation of the Moho between the northern and southern parts and from west to east of the basin.

CSS experiments are 2-D methods applied to 3-D structure, while RF data are 1-D methods applied to 3-D structure. Thus, the compiled CSS/RF data are not properly located in space. Migration is the process of restoring 3-D structures from 1-D or 2-D data elements. Migration of both CSS and RF-derived information elements is based on the general trend of the interface (migration surface) in the vicinity of the information element. The 3-D-migration surface is obtained by an initial interpolation on a coarse grid of 18-km grid spacing, appropriate for the distribution and density of the observed data. Consequently, the information elements are offline migrated perpendicular to the profile in the updipping direction of the initial 3-D-migration surface (see Waldhauser *et al.* 1998, for detailed description). The location of the 3-D-migrated CSS reflector/RF average converter is found by searching for the ray path with incidence perpendicular to the 3-D surface. The velocity in the model is assumed to be constant (ray-theoretical migration, Holliger & Kissling 1991) and, therefore, effects of intracrustal velocity inhomogeneities on the 3-D-migration path are neglected. After the aforementioned migration of all CSS and RF Moho elements, the final interpolation is assessed on a grid resized to $6 \times 6\,\mathrm{km^2}$. This choice is based on evaluation of resolution. Seismic lateral velocity variations are best accommodated by 6 km by 6 km gridding and complemented by a 2-km vertical gridding due to expected stronger velocity variations with depth, in particular, across the Moho.

3.2 Results

In Fig. 10, the overall weighted CSS and RF information used for the interpolation of the Moho topography are shown. In the interpolation procedure, all the CSS and RF Moho information with uncertainties larger than ± 15 km, corresponding to weights of less than 0.2, are neglected. Both CSS and RF information show higher
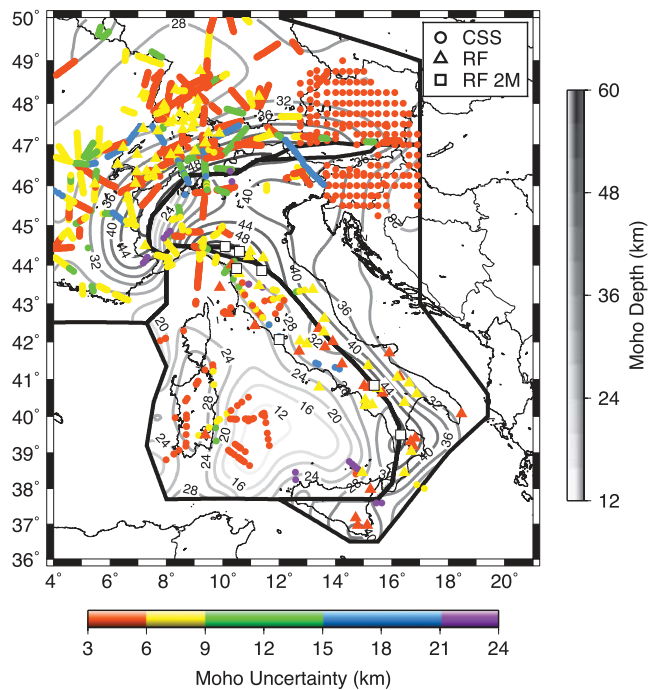

Figure 10. CSS and RF Moho information for the European, Adriatic and Tyrrhenian plates including their relative uncertainties used for the interpolation of the Moho topography (shown as grey scale contours). Circles refer to CSS. Triangles refer to high-quality RF. Squares refer to RF where two Mohos are identified (see text). Note the variable information density and uncertainties in different regions. In general, the plate boundaries are well resolved, but Moho topography within Adriatic and Tyrrhenian plates remains in parts uncertain (see Fig. 11).

Moho uncertainties in regions where the structure is complex, such as near the suture zones (Adria–Tyrrhenia and Europe–Adria). In general, coverage by CSS information within the Alpine region and in its northern foreland is excellent (e.g. Waldhauser *et al.* 2002; Behm 2006; Behm *et al.* 2007; Brueckl *et al.* 2010). In the Italian peninsula, however, CSS profiles are sparse and our model mostly relies on RF information to compensate for the partial lack of CSS information in that region, at least in the continental Tyrrhenian Plate and along the Adria–Tyrrhenia suture zone.

In the northern Alpine region, the interpolated European Moho topography is in general of high quality, based on significant amount of information and with rather low Moho uncertainty. In the Europe–Adria suture zone, resolution and quality of interpolation results are excellent to fair despite the complex structure (e.g. Ivrea body). Along the Adria–Tyrrhenia suture zone, resolution and quality are variable from good to poor. Both Adriatic and Tyrrhenia Moho show regions of high resolution, but are of lower quality in the region of the northern Apennines. High-quality information are present in some spots in the central and southern Apennines regions (Fig. 10). At last, the Tyrrhenian Moho is well resolved in the Sardinia region.

The resulting model of the 3-D interpolation for the Adriatic, Tyrrhenian and European Moho is shown in Fig. 11. The Moho depths obtained in this study are in accordance with the more recent studies in the central Mediterranean region (Waldhauser *et al.* 2002; Behm *et al.* 2007; Di Stefano *et al.* 2009, 2011; Wagner *et al.* 2012). The dominant feature of the Moho in the central Mediterranean region is its strong topography varying between 10 and 60 km. This characteristic is not only present at plate boundaries, but also within the plates, indicating significant ongoing intraplate tectonics and correlating with the complex micro-plate evolution.
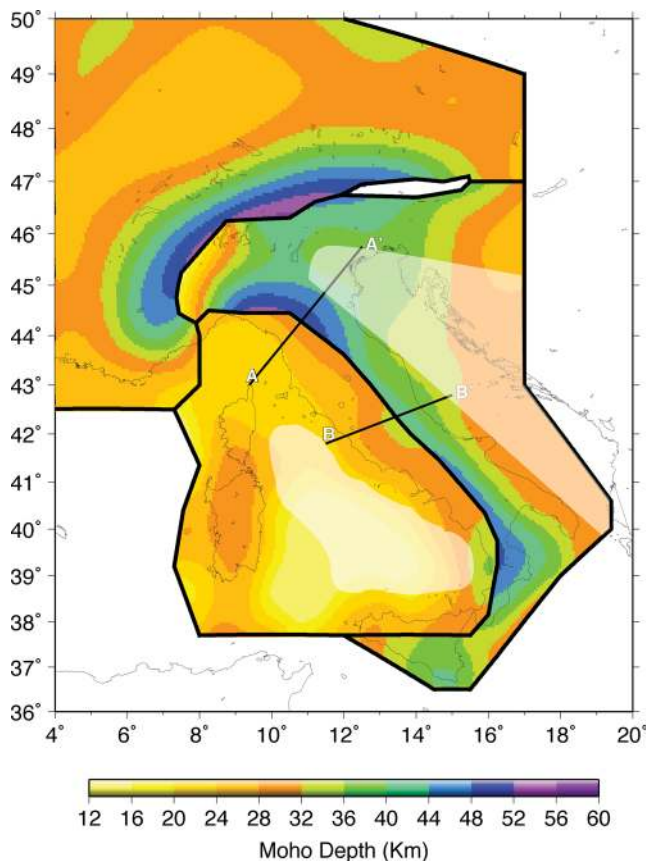
Figure 11. Map describing the Moho topography for the European, Adriatic and Tyrrhenian plates. For regional features, overall uncertainties are generally below ±3 km. Please consult information density presented in Fig. 10 for assessment of local uncertainties. Transparent areas denote regions of reduced reliability of interpolation results due to the presence of no reliable Moho information (supporting points).

The European Moho shows a typical depth of a normal continental crust in the northern Alpine foreland (∼32) km and a distinctively dipping Moho toward SE in the central Alps and toward S in the eastern Alps (Fig. 11). The deepest parts with more than 55 km are observed in the central Alps along the southern plate boundaries (Fig. 11). In the eastern Alps, CSS and RF information show a smoothly shallowing European Moho toward east from about 50 km beneath the Tauern to 32 km at 16°E. Along the western and central Alps, the European Moho descends beneath the Ivrea body and the Adriatic Moho. East of 12.5°E recent CSS data obtained by *PmP* time term analysis (Behm *et al.* 2007) documents a gap between the European and the Adriatic Moho. Outside the Alps the European Moho is rapidly and smoothly shallowing to normal continental crustal depth. Finally, in the western Alps, where CSS and RF information density is somewhat reduced, our Moho map is mainly based on CSS and LET data by Waldhauser *et al.* (1998) and Diehl *et al.* (2009) as combined by Wagner *et al.* (2012).

The Tyrrhenian plate is characterized by different kind of lithospheres (thinned continental to the north and oceanic to the south) in different stages of evolution from north to south and from west to east in the Tyrrhenian Sea (Faccenna *et al.* 2001). In the northern part, we find the Moho at approximately 20 km depth in the region of the Liguro-Provenčal mid oceanic ridge (Fig. 11). From there, Moho is dipping smoothly in southerly direction toward the Corsica-Sardinia continental block. In the southern part, the Tyrrhenian Moho is shallowing to only about 12 km depth in the

area of Marsilli and Vavilov basins (see Fig. 1). Along the plate boundary with Adria beneath the Italian peninsula, the Tyrrhenian Moho shows a significant variation from north to south reaching the maximum depth in the central Apennines and the Calabrian Arc. These results are in general agreement with the interpretation by Di Stefano *et al.* (2009) derived from LET. For a quantitative comparison, however, these LET results would need to be integrated into our model by a process as proposed by Wagner *et al.* (2012).

In the region of the Adriatic Sea, we find a typical depth of the continental crust (∼32 km) for the Adriatic Moho, see Fig. 11. In the continental region, the Adriatic Moho is dipping towards the plate boundary with Tyrrhenia. Greater depths at the plate boundary characterize the northern Apennines and the Calabrian Arc (≥48 km), while in the centre part of the Apennines we observe a maximum of about 40 km. In the north, the Adriatic Moho smoothly dips from a typical young continental depth (∼32 km) along the axis of the P_o plain to 40 km and more in the southern Alps (Fig. 11). Finally, in the west along the Europe–Adria plate boundary the Adriatic Moho marks the top of the Ivrea body shallowing in places to less than 12 km. In this area, our Moho is mostly based on the combination of CSS and LET information as proposed by Wagner *et al.* (2012). These results are in general agreement with previous studies (e.g. Kissling *et al.* 1995; Solarino *et al.* 1997; Bethoux *et al.* 2007; Di Stefano *et al.* 2011).

4 DISCUSSION AND CONCLUSIONS

We propose a new methodology to quantitatively combine CSS and LET (Waldhauser *et al.* 1998; Wagner *et al.* 2012) with RF information to derive high-quality Moho maps for reference 3-D crustal models. We then present a new Moho map of the Alpine–Central Mediterranean region based on CSS, LET and RF seismic data. We introduce a new quality classification/weighting scheme based on uncertainty for RF data, specifically designed to match the criteria proposed in Waldhauser *et al.* (1998) for the CSS information. In a recent study, Di Stefano *et al.* (2011) presented a Moho map for much the same region based on a combination of results of CSS and RF and they applied an qualitative uncertainty estimate scheme for RF data similar to that proposed by Waldhauser *et al.* (1998) for CSS data. While we are using mostly the same original RF data, our methodology to derive quantitative uncertainty estimates for RF information differs significantly and yields less Moho data points but more reliable results as the comparison with independent and coinciding CSS and LET information documents. Thus, the RF assessment methodology proposed here denotes a significant step beyond the one proposed in Di Stefano *et al.* (2011). In particular, Di Stefano *et al.* (2011) employ all backazimuths to derive RF, but in this paper, we subdivide RF information from different backazimuth into different points.

A widely used methodology for RF is the Zhu & Kanamori (2000) method. It is an extension of the grid search method over H (Moho depth) and k (V_p/V_s ratio) proposed by Zandt & Ammon (1995). The method estimates the best H–k combinations by maximizing the sum of the weighted RF amplitudes at the predicted arrival times. This inversion methodology, however, assumes a simple one-layer crustal model with a well-defined horizontal Moho interface. Consequently, in case of such simple crustal structure and very low noise in the signals, the method yields a well-resolved global maxima and the error estimate is reflected in the broadness of the peak. In more realistic cases, however, the methodology has significant problems, showing multiple local maxima (e.g. Eaton *et al.* 2006; Olsson *et al.*

2008). In addition, the results depend on the validity of the chosen range of H and k values since this choice influences the resulting global maximum: a maximum outside of an overly restrictive grid will be excluded while a very liberal grid may include a number of non-physical maxima.

The uncertainty estimation on H–k results are commonly calculated using a bootstrap method (e.g. Efron & Tibshirani 1993). The uncertainty estimation using a bootstrap method, however, is strongly dependent on the signal shape quality. If more than one local maxima is present, the methodology generates high uncertainty depending on the fact that there are several interpretations of the same result and the system is not able to differentiate between them. Furthermore, such kind of inversion results quality estimates is defined as largely independent of the quality of the input data. Hence, for realistic cases, quality of the RF inversion result may not be deduced from inversion fit (e.g. variance reduction) alone. In this study, therefore, we focus on assessment of data uncertainties in combination with their effects on resulting Moho depth uncertainty. In order to provide an approximate quantitative description of the uncertainties of RF results, in a first step we divide, based on quality criteria, the data sets into four different classes. Secondly, for each class, we define an uncertainty value of the Moho depth based on individual observation qualities and on theoretical considerations. In order to define a proper uncertainty value in depth, we consider the vertical resolution of top-quality data for the Moho interface based on Fresnel volume estimates. For the top class (class 0) we estimate an uncertainty of ±3 km based on best physical resolution defined for RF in previous studies (e.g. Lombardi *et al.* 2008). The uncertainty is also related to azimuthal coverage and related effect

on Moho estimation. In fact, a correct and consistent identification of the *Ps* phase is strongly related to the azimuthal coverage and the complexity of the crustal structure, such as the presence of velocity heterogeneities beneath a station (e.g. Lombardi *et al.* 2008). Such effects strongly influence the quality of the *Ps* phase with respect to the first arriving *P*, possibly increasing uncertainty in identification of the *Ps* phase. Even if the classification scheme is subjective, the number of general criteria well define the class of an RF. In fact, the general criteria are correlated to all possible information that can be used to correctly identify the *Ps* phase in RF in order to estimate Moho depth.

To better correlate the uncertainty scheme for RF with the CSS criteria proposed in Waldhauser *et al.* (1998), we compare the RF information with colocated independent LET/CSS information in the region. In general, we find a good correlation, within the uncertainty, between the well-resolved LET Moho (Diehl *et al.* 2009), the CSS Moho and the high-quality RF Moho. Moreover, we find that in cases where we see doubled Moho converters in RF, we are able to correlate them by realistic 3-D migration to the two Moho surfaces Liguria/Tyrrhenia and Adria across the suture zone in the northern Apennines.

The Moho map for the central Mediterranean region is established by interpolating all CSS and high-quality RF information with the criteria proposed by Waldhauser *et al.* (1998) for CSS extended to RF in this study. The map shows strong lateral heterogeneity of Moho depth and a complex interaction between the three main plates (European, Tyrrhenian and Adriatic), confirming results from high-resolution *P*-wave seismic tomography (Diehl *et al.* 2009; Di Stefano *et al.* 2009). The complex tectonics since late Cretaceous
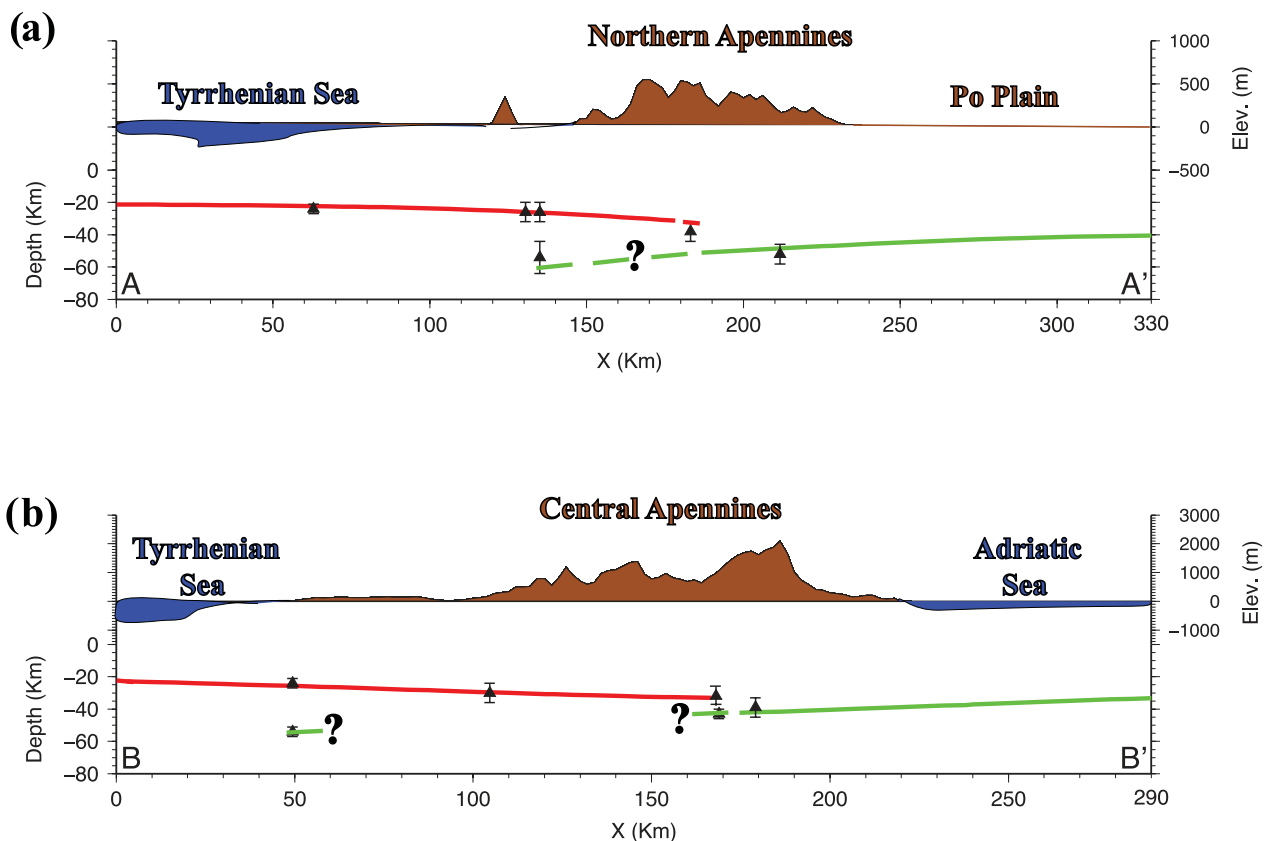

Figure 12. Vertical section through the obtained Moho map (Fig. 11); in red and green we report the depths of the Tyrrhenian, and Adriatic Moho, respectively. Black question marks indicate the not very reliable extrapolated Adriatic Moho underneath the Tyrrhenian Moho. (a) Cros-section A–A′. (b) Cross-section B–B′.

strongly left its marks on continental and oceanic crust, ultimately resulting in the strong lateral undulation of the Moho. The Tethys subduction and the subsequent continental collision created deflections of the European and Adriatic crust down to 50 km in the Alpine and northern Apennines regions. In post-Oligocene times, oceanic and parts of continental Apenninic lithosphere start to subduct beneath the Tyrrhenian plate with different behaviour of the segments along the entire peninsula. This difference is closely connected to the complex geodynamic history of the region and results in variable Moho depth along the suture zone. The observed offset between the Tyrrhenian and the Adriatic Moho is significantly smaller in central Italy with respect to the northern Apennines and the Calabrian Arc (Figs 12 and 13).

The resulting Moho map in large parts shows results similar to those by Di Stefano *et al.* (2011). Significant differences in Moho topography, however, are observed in three regions: (1) in the northern Apennines suture zone the locations and geometries of the complex plate boundaries are now in accordance with all seismic data available in the region, in particular, the recent LET results presented by Diehl *et al.* (2009) and Di Stefano *et al.* (2009). (2) In the Western Alps, the main and significant difference regards the integration of the Ivrea body (Fig. 1) in the Moho topography of the Adria Plate (Wagner *et al.* 2012). (3) The Moho topography in the Eastern Alpine region is significantly different due to the higher density of CSS information with respect to Di Stefano *et al.* (2011) included in this study for the region based on results by (Behm 2006; Behm *et al.* 2007; Brueckl *et al.* 2010).

Based on quality assessment, more than 50 per cent of RF information of the initial data set has been rejected in this study. Hence,
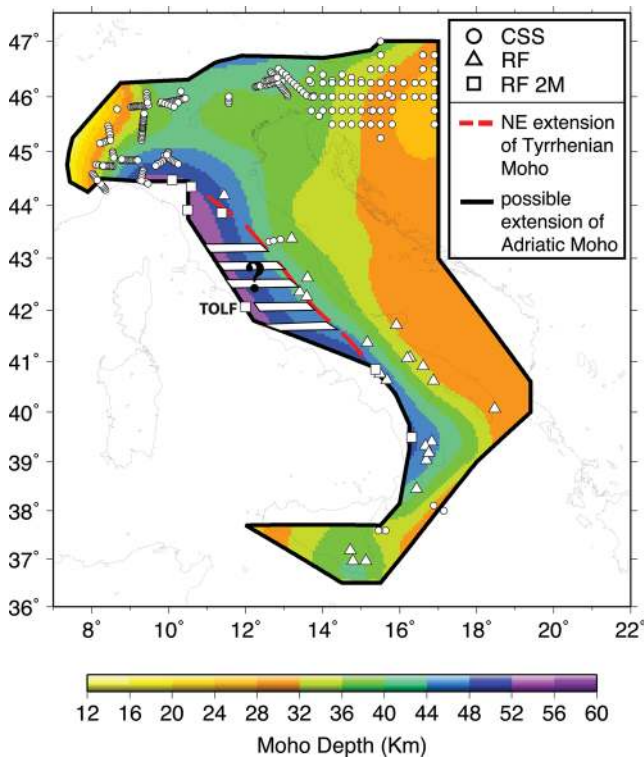
we believe the presented Moho topography to be more reliable than any previous map, of course limited to those areas only, where we have sufficient coverage by high-quality data. Obviously, a significant part of Adria and Tyrrhenia remains poorly sampled (Fig. 11). Hence, we do not propose our map to be an improvement in those particular region.

Further details about the European Moho beneath the Alpine region are given by Kissling *et al.* (2006), Brueckl *et al.* (2010) and Waldhauser *et al.* (1998). For the Tyrrhenian and the Adriatic Moho we refer to Diehl *et al.* (2009) and Di Stefano *et al.* (2011) and for the Ivrea body to Wagner *et al.* (2012). In the subsequent discussion we focus on the northern and central Apennines region only. In order to better understand the relationship between the Tyrrhenian and the Adriatic Moho in those regions we analyse two cross-sections where a number of RF are located (Fig. 12). In both profiles A–A′ (Fig. 12a) and B–B′ (Fig. 12b), we find a very good correlation between the interpolated Mohos and the RF projected along the cross-sections. The presence of RF data showing two Mohos, $X = 135$ km in profile A–A′ (Fig. 12a) and $X = 50$ km in profile B–B′ (Fig. 12b), document the complexity of the area, rising the question about the extent of the Adriatic Moho underneath the Tyrrhenian Moho and on its geodynamical meaning.

The good quality of the RF showing two Mohos, permits us to image an extrapolated Adriatic Moho surface beneath the Tyrrhenian Plate (Fig. 13). The well resolved part is the region defined by the horizontal resolution of the RF, since they are interpolated elements. The region between the Adriatic Moho (in black in Fig. 13) and the Tyrrhenian boundary used in the main interpolation (red dashed line in Fig. 13) is imaged by extrapolation of the data and thus not very reliable (white bars and question mark in Fig. 13). Nevertheless, our results and the speculative interpretation of the two doubled Moho RF data points contribute further to the ongoing discussion about slab geometries and, hence, Moho topography in northern, central and southern Apennines and Calabrian Arc (e.g. Lucente *et al.* 1999; Lucente & Margheriti 2008; Rosenbaum *et al.* 2008; Koulakov *et al.* 2009; Benoit *et al.* 2011).

In recent studies, slab tearing of the Adriatic lithosphere has been proposed (e.g. Rosenbaum *et al.* 2008; Gasparon *et al.* 2009). The presence of a slab tearing at 43°N (e.g. Rosenbaum *et al.* 2008) would indicate a totally independent subduction process between the northern and central parts of the Adriatic plate. The area northern than 43°N (Figs 12a and 13) is shown to be in good correlation with the results of previous studies by ambient noise tomography (e.g. Verbeke *et al.* 2012) and the margin of the northern part of the slab proposed by Benoit *et al.* (2011) in a LET study. It is also the most reliable extrapolated zone thanks to the significant number of high-resolution information we have with respect to the central part of the peninsula. Southern of 43°N our results are not reliable (white bars in Fig. 13) due to the sole presence of one information point (station TOLF of the Italian Seismic Network, Fig. 14). The interpolated point is located at the boarder of the Tuscany and Roman magmatic province at about 42°N (Rosenbaum *et al.* 2008). The RF of the station TOLF of the Italian Seismic Network shows two maximum *Ps* peaks (Fig. 14). In the RF, it is clear that the upper peak belongs to the Tyrrhenian Plate (signals contributing to the maximum peak are from SW), while the lower seems to belong to Adria (signals contributing to the maximum peak are from NE). However, in contrast with this result, RF local studies based on seismic arrays in the area of the TOLF seismic station show only the Tyrrhenian Moho (e.g. Buttinelli 2011), documenting the complexities of local crustal structures. The overlap between Tyrrhenian
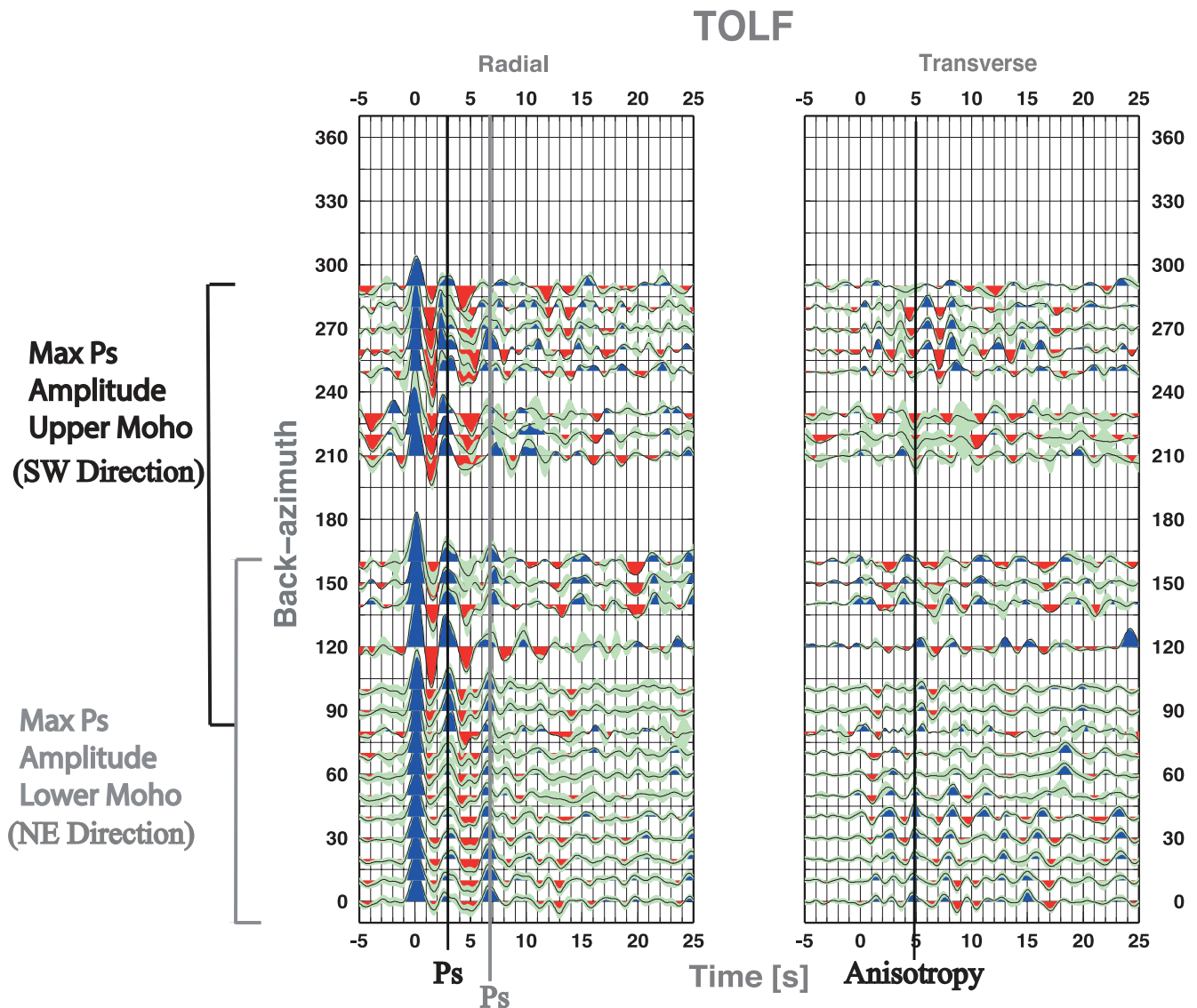

Figure 13. Extrapolated map of Adriatic Moho topography base on class 2M RF information beneath Tyrrhenian Moho. In the region covers in parts by white bands the extrapolation is speculative (e.g. Rosenbaum *et al.* 2008) and it entirely depends on the single class 2M RF point (TOLF station) at 42°N latitude near the coast marked by a square. Along the plate boundary, however, the two Mohos are reliable images (see text and Fig. 11).

Figure 14. Maximum *Ps* amplitude and relative azimuth for the station TOLF of the Italian Seismic Network. On the left the radial component and on the right the transversal component. The two Moho depths are calculated using a $V_p = 6.5 \, \text{km s}^{-1}$ and a $V_p/V_s = 1.725 \, \text{km s}^{-1}$. The black and grey lines show the peak of the two Mohos. The first maximum peak amplitude (black line) is visible between 2.5 and 3 s along 260° BAZ, while the second one (grey line) is visible between 5.5 and 7.5 s along 240° BAZ. The estimated depth is ∼24 and ∼54 km for the upper and the lower Moho, respectively. On the transverse component, the black line indicates where the inversion of the signal is present highlighting the anisotropy. There is a clear inversion from a positive, within 0°–160° BAZ, to a negative, within 210°–280° BAZ, sign of the signal around 5 s. The upper Moho has maximum amplitude of the *Ps* phase in the range between 150° and 300° around 3 s. Thus, the incoming ray path is refracting by the Tyrrhenian Moho. The lower Moho has maximum amplitude of the *Ps* phase in the range between 0° and 100° around 7 s. Thus, the incoming ray path is refracting by the Adriatic Moho.

and Adriatic Moho towards east, along latitude 42°N, is well documented in recent local studies (e.g. Piana Agostinetti *et al.* 2008, 2011; Bianchi *et al.* 2010a), while it is not seen in regional (central Apennines) studies (e.g. Di Bona *et al.* 2008; Chiarabba *et al.* 2010). Thus, the lower *Ps* peak at the station TOLF is difficult to interpret with the information we have at present. From a speculative point of view, it could also be part of a remnant lithosphere slab related to the Adriatic slab break-off (e.g. Rosenbaum *et al.* 2008), or—less likely—an upper mantle interface. The area southern than 42°N was subjected to widespread tear-related magmatic activity and magmatism-induced by break-off of the lithospheric slab in the last 2 Ma (Rosenbaum *et al.* 2008). This result is in accordance with what is shown by Verbeke *et al.* (2012) using ambient noise tomography. In summary, the extrapolated Adria Moho be-

neath the Tyrrhenian Moho, as shown in Fig. 13 south of 42° latitude, is possible but not reliably imaged.

The uncertainty estimate classification method for RF proposed in this study correlates well with the one designed by Waldhauser *et al.* (1998) for CSS. It allows homogeneous elaboration of CSS and RF information combined for the definition of a Moho map. The strength of the RF information permit us to see, in particular cases, double Moho beneath a station. As a consequence, we are able to image the Moho of a subducting lower plate below a clear Moho of the upper plate what is not possible by using CSS only. In fact, the lower Moho, if an upper one exists, is barely or not visible by surface-based seismic methods. Furthermore, the methodology we describe can easily be updated with new CSS and RF information, when available. An increase of high-quality information is requested

to better resolve the Moho map in those areas—central Adria and Tyrrhenia—where no or few data are available. The resulting Moho map denotes the simplest smoothest Moho topography with the least number of separate interfaces that fits all available CSS and RF data within their respective individual uncertainty limits. The Moho map proposed here is self-consistent within the central Mediterranean area unlike, for example, the EPcrust Moho map that is derived by integration of information selected from the literature (Molinari & Morelli 2011) and thus susceptible to offsets at the boundaries between integrated information areas. The Moho map does not only provide new insight in geodynamics of a tectonically active region, but may also serve as starting point in order to build reference 3-D crustal model for high-resolution teleseismic tomography targeting the equally complex lithosphere-astenosphere system beneath Italy.

REFERENCES

Arlitt, R., Kissling, E., Ansorge, J. & Group, T.W., 1999. Three-dimensional crustal structure beneath the TOR array and effects on teleseismic wavefronts, *Tectonophysics,* **314,** 309–319.

Babist, J., Handy, M.R., Konrad-Schmolke, M. & Hammerschmidt, K., 2006. Precollisional, multistage exhumation of subducted continental crust: the Sesia Zone, western Alps, *Tectonics,* **25**(6), TC6008, doi:10.1029/2005TC001927.

Bassin, C., Laske, G. & Masters, G., 2000. The current limits of resolution for surface wave tomography in North America, *EOS, Trans. Am. geophys. Un.,* **81,** F897.

Baumann, M., 1994. Three-Dimensional Modeling of the Crust-Mantle Boundary in the Alpine Region, *PhD thesis,* ETH Zurich, Zurich.

Behm, M., 2006. Accuracy and resolution of a 3D seismic model of the Eastern Alps, *PhD thesis,* Vienna University of Technology, Vienna.

Behm, M., Brueckl, E., Chwatal, W. & Thybo, H., 2007. Application of stacking and inversion techniques to three-dimensional wide-angle reflection and refraction seismic data of the Eastern Alps, *Geophys. J. Int.,* **170**(1), 275–298.

Benoit, M.H., Torpey, M., Liszewski, K., Levin, V. & Park, J., 2011. P and S wave upper mantle seismic velocity structure beneath the northern Apennines: new evidence for the end of subduction, *Geochem. Geophy. Geosyst.,* **12,** Q06004, doi:10.1029/2010GC003428.

Bethoux, N., Sue, C., Paul, A., Virieux, J., Frechet, J., Thouvenot, F. & Cattaneo, M., 2007. Local tomography and focal mechanisms in the south-western Alps: comparison of methods and tectonic implications, *Tectonophysics,* **432,** doi:10.1016/j.tecto.2006.10.004.

Bianchi, I., Chiarabba, C. & Piana Agostinetti, N., 2010a. Control of the 2009 L'Aquila earthquake, central Italy, by a high-velocity structure: a receiver function study, *J. geophys. Res.,* **115,** B12326, doi:10.1029/2009JB007087.

Bianchi, I., Park, J., Piana Agostinetti, N. & Levin, V., 2010b. Mapping seismic anisotropy using harmonic decomposition of receiver functions: an application to Northern Apennines, Italy, *J. Geophys. Res.,* **115,** B12317, doi:10.1029/2009JB007061.

Blundell, D., Freeman, R. & Müller, S., 1992. *A Continent Revealed: The European Geotraverse,* Cambridge University Press, New York.

Brueckl, E., Behm, M., Decker, K., Grad, M., Guterch, A., Keller, G.R. & Thybo, H., 2010. Crustal structure and active tectonics in the Eastern Alps, *Tectonics,* **29,** TC2011, doi:10.1029/2009TC002491.

Buttinelli, M., 2011. 3D reconstruction of crustal structure and volcano-tectonic evolution of Alto Lazio area (Italy): constraints for Geological Storage of CO2, *PhD thesis,* Università degli Studi Roma 3, Rome.

Capitanio, F. & Goes, S., 2006. Mesozoic spreading kinematics: consequences for Cenozoic Central and Western Mediterranean subduction, *Geophys. J. Int.,* **165**(3), 804–816.

Chiarabba, C., Jovane, L. & DiStefano, R., 2005. A new view of Italian seismicity using 20 years of instrumental recordings, *Tectonophysics,* **395,** 251–268.

Chiarabba, C., Bagh, S., Bianchi, I., De Gori, P. & Barchi, M., 2010. Deep structural heterogeneities and the tectonic evolution of the Abruzzi region (Central Apennines, Italy) revealed by microseismicity, seismic tomography, and teleseismic receiver functions, *Earth planet. Sci. Lett.,* **295,** 462–476.

Dercourt, J. *et al.*, 1986. Geological evolution of the Tethys Belt from the Atlantic to the Pamirs since the Lias, *Tectonophysics,* **123,** 241–315.

Di Bona, M., Lucente, F. & Piana Agostinetti, N., 2008. Crustal structure and Moho depth profile crossing the central Apennines (Italy) along the N42 degrees parallel, *J. geophys. Res.-Sol. Earth,* **113,** B12306, doi:10.1029/2008JB005625.

Di Stefano, R., 2005. Subduction-collision structure beneath Italy: high resolution images of the Adriatic-European-Tyrrhenian Litospheric System, *PhD thesis,* ETH Zurich, Zurich.

Di Stefano, R., Kissling, E., Chiarabba, C., Amato, A. & Giardini, D., 2009. Shallow subduction beneath Italy: three-dimensional images of the Adriatic-European-Tyrrhenian lithosphere system based on high-quality P wave arrival times, *J. Geophys. Res.-Sol. Earth,* **114,** B05305, doi:10.1029/2008JB005641.

Di Stefano, R., Bianchi, I., Ciaccio, M.G., Carrara, G. & Kissling, E., 2011. Three-dimensional Moho topography in Italy: new constraints from receiver functions and controlled source seismology, *Geochem. Geophy. Geosyst,* **12**(9), Q09006, doi:10.1029/2011GC003649.

Diehl, T., Husen, S., Kissling, E. & Deichmann, N., 2009. High-resolution 3-D P-wave model of the Alpine crust, *Geophys. J. Int.,* **179**(2), 1133–1147.

Eaton, D., Dineva, S. & Mereu, R., 2006. Crustal thickness and V-P/V-S variations in the Grenville orogen (Ontario, Canada) from analysis of teleseismic receiver functions, *Tectonophysics,* **420**(1–2), 223–238.

Efron, B. & Tibshirani, R., 1993. *An Introduction to the Bootstrap,* Monographs on Statistics & Applied Probability, Chapman & Hall/CRC, New York, NY, USA.

Egloff, R., 1979. Sprengseismische Untersuchungen der Erdkruste in der Schweiz, *PhD thesis,* ETH Zurich, Zurich.

Faccenna, C. & Becker, T., 2010. Shaping mobile belts by small-scale convection, *Nature,* **465**(7298), 602–605.

Faccenna, C., Becker, T., Lucente, F., Jolivet, L. & Rossetti, F., 2001. History of subduction and back-arc extension in the Central Mediterranean, *Geophys. J. Int.,* **145**(3), 809–820.

Faccenna, C., Speranza, F., Caracciolo, F., Mattei, M. & Oggiano, G., 2002. Extensional tectonics on Sardinia (Italy): insights into the arc back-arc transitional regime, *Tectonophysics,* **356**(4), 213–232.

Fry, B., Deschamps, F., Kissling, E., Stehly, L. & Giardini, D., 2010. Layered azimuthal anisotropy of Rayleigh wave phase velocities in the European Alpine lithosphere inferred from ambient noise, *Earth planet. Sci. Lett.,* **297,** 95–102.

Gasparon, M., Rosenbaum, G., Wijbrans, J. & Manetti, P., 2009. The transition from subduction arc to slab tearing: evidence from Capraia Island, northern Tyrrhenian Sea, *J. Geodyn.,* **47**(1), 30–38.

Giese, P., Prodehl, C. & Stein, A., 1976. *Explosion Seismology in Central Europe,* Data and Results, Springer.

Handy, M., Schmid, S., Bousquet, R., Kissling, E. & Bernoulli, D., 2010. Reconciling plate-tectonic reconstructions of Alpine Tethys with the geological-geophysical record of spreading and subduction in the Alps, *Earth. Sci. Rev.,* **102,** 121–158.

Holliger, K. & Kissling, E., 1991. Ray theoretical depth migration—methodology and application to deep seismic-reflection data across the Eastern and Southern Swiss-Alps, *Eclogae Geol. Helv.,* **84**(2), 369–402.

Holliger, K. & Kissling, E., 1992. Gravity interpretation of a unified 2-D acoustic image of the central Alpine collision zone, *Geophys. J. Int.,* **111**(2), 213–225.

Hrubcova, P. & Geissler, W., 2009. The Crust-Mantle transition and the Moho beneath the Vogtland/West Bohemian Region in the light of different seismic methods, *Stud. Geophys. et Geod.,* **53,** 275–294.

Kissling, E., 1993. Deep structure of the Alps–what do we really know?, *Phys. Earth planet. Inter.,* **79,** 87–112.

Kissling, E., Ansorge, J. & Baumann, M., 1997. Methodological considerations of 3-D crustal structure modeling by 2-D seismic methods, in *Deep Structure of Switzerland*. NFP20-Atlas, Swiss National Science Foundation Project 20, pp. 31–38.

Kissling, E., Solarino, S. & Cattaneo, M., 1995. Improved seismic velocity reference model from local earthquake data in Northwestern Italy, *Terra Nova,* **7**(5), 528–534.

Kissling, E., Schmid, S., Lippitsch, R., Ansorge, J. & Fuegenschuh, B., 2006. Litosphere structure and tectonic evolution of the Alpine arc: new evidence from high-resolution teleseismic tomography, *Geol. Soc., Lond., Memoirs,* **32,** 129–145.

Koulakov, I., Kaban, M.K., Tesauro, M. & Cloetingh, S., 2009. P- and S-velocity anomalies in the upper mantle beneath Europe from tomographic inversion of ISC data, *Geophys. J. Int.,* **179**(1), 345–366.

Langston, C., 1979. Structure Under Mount Rainier, Washington, Inferred From Teleseismic Body Waves, *J. geophys. Res.,* **84**(B9), 4749–4762.

Lippitsch, R., Kissling, E. & Ansorge, J., 2003. Upper mantle structure beneath the Alpine orogen from high-resolution teleseismic tomography, *J. geophys. Res.,* **108**(B8), 2376, doi:10.1029/2002JB002016.

Lombardi, D., Braunmiller, J., Kissling, E. & Giardini, D., 2008. Moho depth and Poisson's ratio in the Western-Central Alps from receiver functions, *Geophys. J. Int.,* **173**(1), 249–264.

Lucente, F., Chiarabba, C., Cimini, G. & Giardini, D., 1999. Tomographic constraints on the geodynamic evolution of the Italian region, *J. geophys. Res.-Sol. Earth,* **104**(B9), 20307–20327.

Lucente, F.P. & Margheriti, L., 2008. Subduction rollback, slab breakoff, and induced strain in the uppermost mantle beneath Italy, *Geology,* **36**(5) 375–378.

Malinverno, A. & Ryan, W., 1986. Extension in the Tyrrhenian Sea and Shortening in the Apennines as result of Arc Migration driven by sinking of the lithosphere, *Tectonics,* **5**(2), 227–245.

Margheriti, L. *et al.*, 2006. The subduction structure of the Northern Apennines: results from the RETREAT seismic deployment, *Ann. Geophys.,* **49**(4–5), 1119–1131.

Mele, G. & Sandvol, E., 2003. Deep crustal roots beneath the northern Apennines inferred from teleseismic receiver functions, *Earth planet. Sci. Lett.,* **211,** 69–78.

Molinari, I. & Morelli, A., 2011. EPcrust: a reference crustal model for the European Plate, *Geophys. J. Int.,* **185**(1), 352–364.

Mooney, W., Laske, G. & Masters, T., 1998. CRUST 5.1: A global crustal model at 5 degrees × 5 degrees, *J. geophys. Res.,* **103**(B1), 727–747.

Olsson, S., Roberts, R. & Bodvarssoni, R., 2008. Moho depth variation in the Baltic Shield from analysis of converted waves, *Gff,* **130**(3), 113–122.

Peng, X. & Humphreys, E., 1997. Moho dip and crustal anisotropy in Northwestern Nevada from teleseismic receiver functions, *Bull. seism. Soc. Am.,* **87**(3), 745–754.

Piana Agostinetti, N. & Amato, A., 2009. Moho depth and V-p/V-s ratio in peninsular Italy from teleseismic receiver functions, *J. geophys. Res.-Sol. Earth,* **114,** B06303, doi:10.1029/2008JB005899.

Piana Agostinetti, N., Park, J. & Lucente, F.P., 2008. Mantle wedge anisotropy in Southern Tyrrhenian Subduction Zone (Italy), from receiver function analysis, *Tectonophysics,* **462,** 35–48.

Piana Agostinetti, N., Bianchi, I., Amato, A. & Chiarabba, C., 2011. Fluid migration in continental subduction: the Northern Apennines case study, *Earth planet. Sci. Lett.,* **302**(3–4), 267–278.

Reilinger, R. *et al.*, 2006. GPS constraints on continental deformation in the Africa-Arabia-Eurasia continental collision zone and implications for the dynamics of plate interactions, *J. geophys. Res.,* **111**(B05411), doi:10.1029/2005JB004051.

Rosenbaum, G., Gasparon, M., Lucente, F.P., Peccerillo, A. & Miller, M., 2008. Kinematics of slab tear faults during subduction segmentation and implications for Italian magmatism, *Tectonics,* **27**(2), TC2008, doi:10.1029/2007TC002143.

Sandoval, S., Kissling, E., Ansorge, J. & Group, S.S.T.W., 2003. High-Resolution body wave tomography beneath the SVEKALAPKO array: I. A priori three-dimensional crustal model associated traveltime effects on teleseismic wave fronts, *Geophys. J. Int.,* **153,** 75–87.

Savage, M., 1998. Lower crustal anisotropy or dipping boundaries? Effects on receiver functions and a case study in New Zealand, *J. geophys. Res.,* **103**(B7), 15069–15087.

Scrocca, D., Doglioni, C., Innocenti, F., Manetti, P., Mazzotti, A., Bertelli, L., Burbi, L. & D'Offizzi, S., 2003. CROP ATLAS—seismic reflection profiles of the Italian Crust, *Mem. Descr. Carta. Geol. It.,* **62**.

Sheriff, R. & Geldart, L., 1995. *Exploration Seismology,* Cambridge University Press, New York.

Solarino, S., Kissling, E., Cattaneo, M. & Eva, C., 1997. Local earthquake tomography of the southern part of the Ivrea body, North-Western Italy, *Eclogae Geol. Helv.,* **90**(2), 357–364.

Verbeke, J., Boschi, L., Stehly, L., Kissling, E. & Michelini, A., 2012. High-resolution Rayleigh-wave velocity maps of central Europe from a dense ambient-noise data set, *Geophys. J. Int.,* **188**(3), 1173–1187.

Wagner, M., Kissling, E. & Husen, S., 2012. Combining controlled-source seismology and local earthquake tomography to derive a 3D crustal model of the western Alpine region, *Geophys. J. Int.,* **191,** 789–802.

Waldhauser, F., 1996. A parametrized three-dimensional Alpine Crustal Model and its application to teleseismic wavefront scattering, *PhD thesis,* ETH Zürich.

Waldhauser, F., Kissling, E., Ansorge, J. & Mueller, S., 1998. Three-dimensional interface modelling with two-dimensional seismic data: the Alpine crust-mantle boundary, *Geophys. J. Int.,* **135,** 264–278.

Waldhauser, F., Lippitsch, R., Kissling, E. & Ansorge, J., 2002. High-resolution teleseismic tomography of upper-mantle structure using an a priori three-dimensional crustal model, *Geophys. J. Int.,* **150,** 403–414.

Ye, S., Ansorge, J., Kissling, E. & Mueller, S., 1995. Crustal structure beneath the Eastern Swiss Alps derived from Seismic-refraction data, *Tectonophysics,* **242,** 199–221.

Yilmaz, O., 2001. *Seismic Data Analysis,* 2nd edn, Vol. 2, Society of Exploration Geophysicists, Tulsa, OK, USA.

Zandt, G. & Ammon, C., 1995. Continental crust composition constrained by measurements of crustal Poisson's ratio, *Nature,* **374,** 152–154.

Zhu, L. & Kanamori, H., 2000. Moho depth variation in southern California from teleseismic receiver functions, *J. geophys. Res.,* **105**(B2), 2969–2980.

SUPPORTING INFORMATION

Additional Supporting Information may be found in the online version of this article:

Table S1. RF Moho depth and classification used in this study. Moho depth estimated using an average $V_p = 6.5\,\mathrm{km\,s^{-1}}$ and an average $V_p/V_s = 1.725\,\mathrm{km\,s^{-1}}$, see text for explanation. For station in *class 4,* in the Moho depth column, the estimated Moho and, in italic, the possibly intracrustal feature depths including uncertainties are shown. For station in *class 2M,* in the Moho depth column, estimated depths for the upper and lower Moho including uncertainties are shown. Data sets: Piana Agostmetti and Amato (2009)[1]; Lombardi *et al.* (2008)[2]. In the latter only the classification has been performed, Moho depth estimation are from Lombardi *et al.* (2008), see text (http://gji.oxfordjournals.org/lookup/suppl/doi:10.1093/gji/ggt148/-/DC1)

Please note: Oxford University Press are not responsible for the content or functionality of any supporting materials supplied by the authors. Any queries (other than missing material) should be directed to the corresponding author for the article.